

**STOCHASTIC MODELING OF THE CELL KILLING EFFECTS OF
LOW AND HIGH LET RADIATION**

A Thesis

by

JULIEN PARTOUCHE

Submitted to the Office of Graduate Studies of
Texas A&M University
in partial fulfillment of the requirements for the degree of

MASTER OF SCIENCE

December 2004

Major Subject: Health Physics

**STOCHASTIC MODELING OF THE CELL KILLING EFFECTS OF
LOW AND HIGH LET RADIATION**

A Thesis

by

JULIEN PARTOUCHE

Submitted to Texas A&M University
in partial fulfillment of the requirements
for the degree of

MASTER OF SCIENCE

Approved as to style and content by:

Dan Reece
(Chair of Committee)

John Ford
(Member)

Leslie Braby
(Member)

Michael Walker
(Member)

William Burchill
(Head of Department)

December 2004

Major Subject: Health Physics

ABSTRACT

Stochastic Modeling of the Cell Killing Effects of
Low and High LET Radiation. (December 2004)
Julien Partouche, Diplôme d'ingénieurs, Fondation EPF
Chair of Advisory Committee: Dr. Dan Reece

Theoretical modeling of biological response to radiation describes qualitatively and quantitatively the results of radiobiological effects at the molecular, chromosomal, and cellular level. The repair-misrepair (RMR) model is the radiobiological model chosen for our study. It models deoxyribonucleic acid (DNA) damage formation and lesion repair through linear and quadratic processes.

Double strand breaks (DSB) are a critical lesion in DNA. With increasing LET, the number of DSB per track traversing the cell nucleus increases. Using a compound Poisson process (CPP), we describe DNA damage formation. Three models were considered: a simple CPP using constant LET, a CPP using a chord length distribution, and a CPP using specific energy distribution. In the two first cases, and for low LET radiation the initial distribution of DSB was well approximated by a Poisson distribution, while for high LET radiation the initial distribution of DSB deviated slightly from a Poisson distribution. In the last case, DSB distribution was much broader than a pure Poisson distribution.

Datasets from the literature for seven human cell lines, exhibiting various sensitivities to radiation were analyzed.

We compared stochastic, CPP, and CPP using chord length distribution, with deterministic RMR models. For low LET radiation and at high dose rates the stochastic survival results agree well with the deterministic survival results. Also the stochastic model allows for non-linearity at low doses due to the accumulation of sub-lethal damage. At low dose rates deterministic results overestimate the surviving fraction compared to stochastic results. For high LET radiation stochastic and deterministic survival results agree. Stochastic survival results using specific energy distribution

diverged from deterministic results by underestimating the surviving fraction at low and high LET radiation.

The dose rate sparing curve, representing surviving fraction at a dose of 10Gy vs. dose rate shows that deterministic survival results are consistent with stochastic survival results, using CPP, or CPP with chord length distribution, for low and high dose rate values. Compared to deterministic aspects of DNA damage formation we concluded that stochastic aspects of DNA damage formation and repair using CPP or CPP with chord length distribution are not as prominent as reported in the earlier studies.

ACKNOWLEDGMENTS

First, I would like to thank Dr. Dan Reece for his help throughout all aspects of the work and for permitting me to come to Texas A&M University. Without his continuous support, this effort would not have been possible.

Sincere gratitude is extended to my committee, Drs. Leslie Braby, John Ford and Michael Walker.

Drs. Leslie Braby and John Ford particularly deserve great appreciation for the enthusiasm they add in everything they do and for their great knowledge in radiation biology and microdosimetry.

I also would like to thank my mentor, Dr. Robert Stewart, to whom I owe my most sincere appreciation especially for the passion he inserts in everything he does and for his constant help throughout all aspects of the work and the patience he had in advising me.

I would like to thank my family, my father Roger Partouche, and my mother Jacqueline Partouche, my brother Laurent, and my sister Judith for their love and trust. Without them this accomplishment would have been unachievable.

TABLE OF CONTENTS

	Page
ABSTRACT	iii
ACKNOWLEDGMENTS	v
TABLE OF CONTENTS	vi
LIST OF FIGURES	vii
LIST OF TABLES	x
INTRODUCTION AND THEORY	1
Objective and motivation	1
DNA radiation damage	2
Radiobiological models	5
Project overview	6
RMR MODEL	8
Description of the RMR model	8
Deterministic RMR model	14
Stochastic RMR model	19
RESULTS AND DISCUSSION	29
Test of the initial DSB distribution	29
Analytical verification	35
Evaluating the accuracy of SRM software	38
CONCLUSIONS	49
REFERENCES	52
VITA	56

LIST OF FIGURES

	Page
FIG. 1. Various types of DNA damage that could be caused by ionizing radiation. (N) Normal double strands of DNA, (A) Base deletion, (B) Change of base, (C) Dimer, (D) Cross link, (E) Single strand break, (F) Double strand break.	4
FIG. 2. Example of a chromosome aberration, caused by two DSBs. (A) Two chromatids undergoing DSBs. (B) Dicentric aberration. (C) Translocation aberration.	10
FIG. 3. Summary of the RMR model. An important feature of the RMR model is that it considers several endpoints, linear repair, linear misrepair, quadratic repair, quadratic misrepair, and fixation.	12
FIG. 4. Pattern of the DSB deposition in time for the deterministic model, with $nstep=td/\delta_t$	15
FIG. 5. CPP for the energy deposition inside a site at a specified dose. On (A) several tracks or events are going through the cell. Dots on (B) represent ionizations.	22
FIG. 6. Diagram illustrating the variation in the chord length distribution within the site of interest. In a sphere of diameter d the chord length distribution, $f(l)$ is triangular.	24
FIG. 7. Diagram describing four classes of tracks: crossers, particles going all the way through the cell nucleus; stoppers, particles stopping inside the cell nucleus; starters, secondary particles initiated inside the cell nucleus and leaving the cell nucleus; and insiders, secondary particles initiated and stopping inside the cell nucleus.	25
FIG. 8. Lineal energy distribution for a spherical tissue region of one micrometer in diameter for (—) ^{60}Co gamma radiation, and for (--) 15MeV neutrons.	26
FIG. 9. DSBs probability distribution for $\bar{z}_1=0.001\text{Gy}$ and $D=1\text{Gy}$, corresponding to low LET radiation. (■) probability distribution of the number of DSBs predicted with a CPP. (▲) probability distribution of the number of DSBs predicted with a CPP and taking into account the chord length distribution. (■) $\bar{x}=24.9696$, and $\sigma=5.07784$. (▲) $\bar{x}=27.2652$ $\sigma=7.23698$	31

- FIG. 10. DSBs probability distribution for $\bar{z}_1=0.1\text{Gy}$ and $D=1\text{Gy}$, corresponding to low LET radiation. (■) probability distribution of the number of DSBs predicted with a CPP, (▲) probability distribution of the number of DSBs predicted with a CPP and taking into account the chord length distribution. (■) $\bar{x}=2.0819$, and $\sigma=9.32098$. (▲) $\bar{x}=25.98745$, and $\sigma=12.74987$32
- FIG. 11. DSBs probability distribution for low LET radiation and $D=1\text{Gy}$, corresponding to low LET radiation. (■) probability distribution of the number of DSBs predicted with a CPP, (▲) probability distribution of the number of DSBs predicted with a CPP and taking into account the specific distribution. Specific energy distribution is taken from ICRU#36 (33) for Co-60 gamma radiation. (■) $\bar{x}=24.9696$, and $\sigma=5.07784$. (▲) $\bar{x}=28.77401$ $\sigma=16.74982$33
- FIG. 12. DSBs probability distribution for high LET radiation and $D=1\text{Gy}$, corresponding to low LET radiation. (■) probability distribution of the number of DSBs predicted with a CPP, (▲) probability distribution of the number of DSBs predicted with a CPP and taking into account the specific distribution. Specific energy distribution is taken from ICRU#36 (33) for 15 MeV neutron. (■) $\bar{x}=24.9696$, and $\sigma=5.07784$. (▲) $\bar{x}=30.74568$ $\sigma=27.52036$35
- FIG. 13. Comparison of stochastic (●), deterministic (■), and analytical (▲) results for a selected case, i.e. with the binary misrepair term set to zero. Dose rate is equal to 0.34 Gy/h.36
- FIG. 14. Comparison of stochastic (●), deterministic (■), and analytical (▲) results for a selected case, i.e. with the binary misrepair term set to zero. Dose rate is equal to 81 Gy/h.37
- FIG. 15. Comparison of survival results for various low dose rate, 0.24Gy/h and 0.71Gy/h, and high dose rate, 81Gy/h, for low LET radiation, 0.01keV/ μm , and for cell line AG01522. (●) Surviving fraction measured by experiments. (▲) Surviving fraction predicted by deterministic RMR model. (■) Surviving fraction predicted by stochastic RMR model. (×) Surviving fraction predicted by stochastic RMR model taking into account the chord length distribution. (○) Surviving fraction predicted by stochastic RMR model taking into account the specific energy distribution.39

- FIG. 16. Comparison of survival results for several cell lines: (A) A549, (B) HeLa, (C) HX118, and (D) M10. (●) Surviving fraction measured by experiments. (▲) Surviving fraction predicted by deterministic RMR model. (■) Surviving fraction predicted by stochastic RMR model. (×) Surviving fraction predicted by stochastic RMR model taking into account the chord length distribution. (○) Surviving fraction predicted by stochastic RMR model taking into account the specific energy distribution.41
- FIG. 17. Comparison of survival results for high LET radiation, and for cell line SQ20B. Results are presented for a dose rate of 81Gy/h and particle LET of 19.8keV/μm. (●) Surviving fraction predicted by experiments. (▲) Surviving fraction predicted by deterministic RMR model. (■) Surviving fraction predicted by stochastic RMR model. (×) Surviving fraction predicted by stochastic RMR model taking into account the chord length distribution. (○) Surviving fraction predicted by stochastic RMR model taking into account the specific energy distribution.42
- FIG. 18. Effects of fluctuations on dose rate sparing for low LET radiation, for cell line AG01522. All curves show surviving fraction vs. dose rate at a dose of 10Gy. (—) Surviving fraction predicted by the RMR model (--) Surviving fraction predicted by the RMR model with parameter ϕ set to 0. (▲) Surviving fraction predicted by the deterministic RMR model. (■) Surviving fraction predicted by the stochastic RMR model.45
- FIG. 19. Effects of fluctuations on dose rate sparing for high LET radiation, for cell line SQ20B. All curves show surviving fraction vs. dose rate at a dose of 10Gy. (—) Surviving fraction predicted by the RMR model (--) Surviving fraction predicted by the RMR model with parameter ϕ set to 0. (▲) Surviving fraction predicted by the deterministic RMR model. (■) Surviving fraction predicted by the stochastic RMR model.46
- FIG. 20. Effects of fluctuations on dose rate sparing for several cell lines: (A) A549, (B) HeLa, (C) HX118, and (D) M10. All curves show surviving fraction vs. dose rate at a dose of 10Gy. (—) Surviving fraction predicted by the RMR model (--) Surviving fraction predicted by the RMR model with parameter ϕ set to 0. (▲) Surviving fraction predicted by the deterministic RMR model. (■) Surviving fraction predicted by the stochastic RMR model. A, B, and C are for Co-60 exposures; D is for 15 MeV neutrons.48

LIST OF TABLES

	Page
Table I RMR parameters for all types of cells used in the calculation.	19
Table II Comparison of the Poisson distribution associated moments with the exact solutions of the associated moments generated using Monte Carlo method with CPP, CPP considering chord length distribution, and CPP considering specific energy distribution.	30

INTRODUCTION AND THEORY

Objective and motivation

The goal of radiotherapy is to maximize tumor-cell killing and to minimize normal tissue damage. Radiobiological models can be incorporated into radiotherapy treatment planning; for example, reliable prediction of radiotherapeutic isoeffect doses is needed when the temporal exposure pattern is changed (1).

Each normal and malignant tissue has its own radiobiological properties and biological parameters, and the response of normal and tumor tissues depends on the temporal pattern of radiation delivery (e.g., dose rate and dose fractionation). Tumor and tissue responses also depend on LET. Improving the outcome from radiation therapy through radiobiological models will increase clinical relevance of applied radiobiology. One radiobiological model is the RMR model (2). Formulated in terms of the average number of unrepaired and lethally mis-repaired lesions in a cell, the RMR model uses statistical approximations.

The stochastic RMR, model using a probability distribution of unrepaired lesions, and the deterministic RMR model, using average number of unrepaired lesions in a cell, can then be compared to evaluate the accuracy of the non-stochastic RMR model as a function of dose, dose rate, and LET.

Past model intercomparison studies (3, 4, 5) used radiosensitivity parameters that are not necessarily representative of those expected for typical mammalian cells. The particular radiosensitivity parameters used in these studies tended to amplify the stochastic aspects of DNA damage formation and repair processes. The proposed model intercomparison studies, which use representative radiosensitivity parameters determined from measured data, model stochastic aspects of DNA damage formation and repair.

This thesis follows the style and format of *Radiation Research*.

DNA radiation damage

Over the past 50 years radiobiological studies have shown that the effects of ionizing radiation on cells are primarily initiated by the modifications of DNA (6). A crucial advance in the 1940s was the identification of DNA as a carrier of the genetic information (7). DNA is contained inside the nucleus of the cell and consists of a double-stranded helix. Each strand is polynucleotide chain composed of four types of nucleotide subunits (adenosine, thymine, guanine, and cytosine). Nucleotides are nitrogen-containing molecules linked together by the sugar-phosphate “backbone”. Adenine is coupled with thymine, and guanine with cytosine through hydrogen bonds. The two polynucleotide strands bound together form the double helix of DNA. If a typical DNA molecule is stretched to its full length it would be about 1 m long. Storing such a long molecule in a 10 μ m diameter mammalian cell nucleus is possible because of DNA packing from DNA double helix to chromosome.

Cells cycle through an ordered set of phases leading to cell growth and division into two progeny cells. The phases are G₁, S, G₂, and M. The G₁ stage stands for "GAP 1". The S stage stands for "Synthesis". This is the stage when DNA replication occurs. The G₂ stage stands for "GAP 2". The M stage stands for "mitosis", and is when nuclear (chromosomes separation) and cell membrane (cytoplasmic) division occur. Mitosis is typically divided further into 4 phases (prophase, metaphase, anaphase, and telophase) or more. The transmission from one phase to another is under the control of a set of proteins able to delay or arrest the cell cycle progression at several points known as “checkpoints”. If all conditions are satisfied the next phase can be initiated.

When dealing with radiation-induced damage, the presence of DNA damage provokes the activation of “DNA damage sensor proteins” such as ATM, DNA-PK, PARP, and p53 (8). The main checkpoints of interest usually observed in cells exposed to low and high LET radiation are G₁/S, S, and G₂/M. Depending on the severity of the

damage, these proteins will allow the cell cycle to pause, repair and then continue, or, in case of lethal damage, to engage programmed cell death (9).

Ionizing radiations are generally characterized by their ability to excite and ionize atoms of matter with which they interact. Since the energy needed to cause a valence electron to escape an atom is about 30 eV, radiations must carry kinetic or quantum energies in excess of this magnitude to be called “ionizing”(10). Also, as can be seen from Eq. (1), this criterion would seem to include electromagnetic radiation with wavelengths up to about 40 nm, which does not include most of the ultraviolet (UV) radiation band (~10-400 nm).

$$E_{\gamma} = h\nu = \frac{hc}{\lambda} = \frac{1.2398}{\lambda} \quad (1)$$

However, for practical purposes these marginally ionizing UV radiations are not usually considered in the context of radiological physics, since they are even less capable of penetrating through matter than visible light, while other ionizing radiations are generally more penetrating (10).

DNA can either be directly damaged by radiation or indirectly through the action of radicals formed by radiation. During indirect transfer ionizing radiation interacts with materials surrounding the substrate, generating radical species. Water, being the principal constituent of biological systems, is the site for a process called water radiolysis leading to the production of highly reactive compounds such as $^{\circ}\text{OH}$, e^{-}_{aq} , $^{\circ}\text{H}$, H_3O^{+} . Those free radicals, as they are also called, can damage many constituent molecules, among them DNA. In addition radiation interacts directly with DNA leading to either excitation or ionization. The relative importance of direct and indirect energy deposition depends on the nature of the radiation, the particle’s LET, DNA hydration, and the organization of DNA (8).

Different types of damage in the chromatin, from a “gentle” base deletion to a more severe DSB can occur. They are represented in FIG. 1. A single-strand break (SSB), dimer or intra-strand cross-link, base modification, and DNA-protein cross-link

are other common DNA damage caused by radiation. A SSB is a break in the sugar bond between the backbone and the base, and a DSB is a pair of SSB within 10 to 20 base pairs (11). A strand break occurs whenever the deoxyribose sugar is damaged and when the phosphate group that acts as a bridge between adjacent deoxyribose sugars is severed. There are many different kinds of SSB (e.g., a strand break with a base damage on the opposing strand is still a SSB). Without damage to neighboring groups, those types of lesions are called “singly damaged sites” (12).

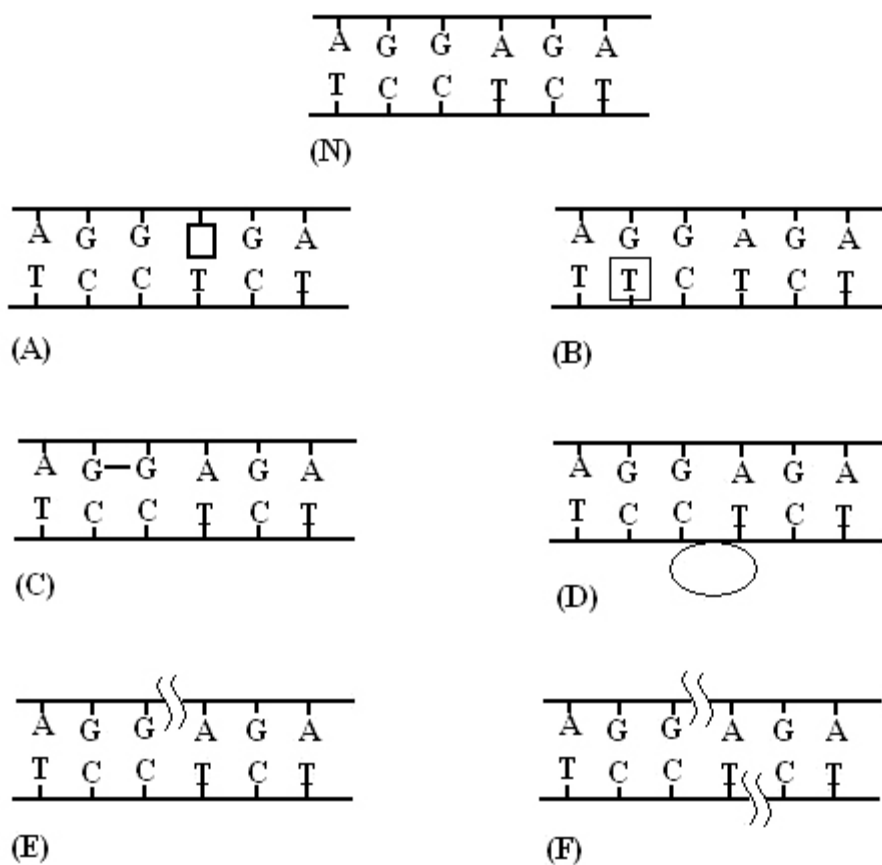


FIG. 1. Various types of DNA damage that could be caused by ionizing radiation. (N) Normal double strands of DNA, (A) Base deletion, (B) Change of base, (C) Dimer, (D) Cross link, (E) Single strand break, (F) Double strand break.

Compared to the so-called “singly damaged sites” we can also distinguish “locally multiply damaged sites”, which corresponds to the presence of several damage sites in a localized region. “Locally multiply damaged sites” are mostly caused by high LET radiation (13).

Associated with DNA damages are repair pathways. Base excision repair (BER) is usually associated with the change of one base (there are two modes of BER: short-patch and long patch), the vast majority of “small” lesions are repaired by the BER pathway and nucleotide excision repair (NER) is usually associated with the changes of three to twenty bases (12). Intra-strand cross-links, and dimers are removed by NER. SSB can be generally repaired generally with ligation. Finally DSB can be rejoined by different pathways such as homologous recombination (HR), non-homologous recombination (NHR), and non-homologous end joining (NHEJ). NHEJ and NHR are highly mutagenic while HR is potentially an error-free DSB repair mechanism. Repair or misrepair mechanisms will often decide the fate of the cell, and kinetic models such as the RMR model, can be used to predict some key aspects of the formation and repair of DNA damage. DSB is widely accepted as the main type of DNA damage responsible for radiation-induced cell killing (14). Following misrepair of a DSB, the main chromosome aberrations that cause instability and possibly death to the cell are acentric ring, acentric fragments, dicentrics, polycentrics, and chromosomal rings (15). Production of such kinds of lethal aberrations occurs with interaction of two DSB.

Radiobiological models

Energy deposition occurs within 10^{-15} s, and chemical changes within 10^{-6} s. Thereafter, enzymatic repair occurs within 10^2 s to 10^4 s. Because repair processes occur much slower than the physiochemical processes responsible for damaging the DNA, damage formation can be regarded as instantaneous compared to the repair kinetics. Kinetic models attempt to relate the temporal evolution of the number of DSB and lethal lesions to higher endpoints such as the fraction of the cells that survive irradiation, also called the surviving fraction. The surviving fraction at time t can be defined as the

fraction of cells without any lethal lesions at a time t (16) and will be the endpoint of interest in our study. Radiobiological models also have impact on mutagenesis as they can help tracking the rate at which mutations accumulate depending on the dose and the dose rate.

Several models have been proposed (2,17,18) This work focuses on one representative kinetic model, the Repair Misrepair (RMR) model (2).

Project overview

In the thesis we present the implementation of the RMR model, based on a mathematical and radiobiological description of the RMR parameters. It also describes the general procedure used to compute the RMR model. Then we describe the deterministic RMR model: we explain how DSB are deterministically computed, and also how we obtain the input for the RMR model. For that input we used the VC software to calibrate the RMR model, and get the radiobiological parameters value for several kinds of radiobiological datasets. The deterministic RMR model is formulated in terms of the average of numbers of unrepaired and lethally mis-repaired DSB in a cell. The central question is, are those mean values a good enough approximation?

To answer this question we developed a stochastic RMR model (SRM) to model better of the stochastic processes going on within a cell nucleus hit by radiation. We describe the stochastic aspects of DNA damage formation via microdosimetric concepts through three different models: a compound Poisson process (CPP) considering LET constant, a CPP considering chord length distribution, and a CPP considering typical specific energy distribution. Then we present the computational implementation of the SRM.

After that we present results obtained with the SRM software. First we compare DSB distribution for a pure Poisson distribution with each of the three stochastic models, CPP considering LET constant, CPP considering chord length distribution, and CPP considering typical specific energy distribution. Second we compare SRM results with analytical solutions on selected problems. Then we evaluate the accuracy of the non-

stochastic RMR model by comparing cell surviving fractions as a function of dose, dose rate and LET. Tests of model accuracy are performed using the representative biological parameters identified with the deterministic VC software. This last section also presents dose rate sparing curves and explains the influence of the dose rate in the survival calculations, comparing results from non-stochastic model and SRM.

The last section contains the conclusions and suggestions for future work.

RMR MODEL

Description of the RMR model

Mathematical description

The RMR model links radiation damage to higher-level end points, such as the surviving fraction, through first- and second-order repair mechanisms. The RMR model is broadly consistent with the breakage and union theory of chromosome aberration formation (15, 16). The RMR model is defined by the following system of coupled, non-linear differential equations (2):

$$\frac{d}{dt} \bar{X}_{DSB}(t) = \dot{D}(t) \Sigma_{DSB} - \lambda \bar{X}_{DSB}(t) - \eta \bar{X}_{DSB}(t) \bar{X}_{DSB}(t) \quad (2)$$

$$\frac{d}{dt} \bar{L}(t) = (1-a_0) \varphi \lambda \bar{X}_{DSB}(t) + \gamma \eta \bar{X}_{DSB}(t) \bar{X}_{DSB}(t) \quad (3)$$

Again the RMR model considers DSB as the lesion of primary interest. \dot{D} is the absorbed dose rate at a cell, expressed in Gy/h, and Σ_{DSB} is the number of DSB created per Gy per cell. RMR model proposes that lesions undergo either linear or quadratic repair. λ represents the linear rate of repair of DSB, and is expressed in hour⁻¹. First order repair may correspond to the chromosome broken-ends rejoining rate by enzymatic processes.

It is useful to relate the repair probability λ to the expected DSB repair half-time τ , which is the expected amount of time required for a cell to remove (repair or misrepair) half of the DSB initially produced in a cell by an acute dose of radiation. For first order rejoining kinetics, we have the expression of λ in Eq. (4), (18):

$$\lambda = \frac{\ln 2}{\tau} \quad (4)$$

DSB can also be removed through quadratic repair pathway. It consists of the interaction of two DSB. η represents the DSB-DSB interaction rate, and is expressed in hour^{-1} . Equation 2 describes the evolution of the number of DSB, \bar{X}_{DSB} , in a cell. The RMR model also describes the evolution of the number of lethal lesions, \bar{L} , in a cell, Eq. (3). In the RMR model, not only must a lesion be repaired, but the repair must also be correct. Repair processes are considered having a probability of success or failure. Linear misrepair has a probability of $(1-a_0)$. Though, it is now widely thought that NHEJ is the main pathway for repairing DSB (19). HR occurs by homology-search process to repair DSB and without any loss of genetic information. This type of search is very hard if the break happens to be in the portion of the genome which is repetitive and roughly 40% of the human genome is repetitive. On one hand during late S, G2, and M phases of the cell cycle, a sister chromatid is optimally positioned physically, HR almost never happens during G0, G1 and early S phases, before replication. These facts taken at face value suggest that HR rarely happens. On the other hand there is some evidence that HR may be an important DSB mechanism during the late S phase and perhaps early G2 (19). That is the quadratic misrepair probability is be equal to one, as any interaction between two different DSB is not a correct repair.

Misrepair leads to the formation of chromosome aberrations and these aberrations are related to cell killing. The RMR model considers that cells can die through lethal misrepair. Not only can a lesion be misrepaired, but the misrepair is considered to be either lethal or not lethal. The RMR model sets ϕ as the fraction of linear lethal misrepair, and γ as the lethal fraction of binary misrepair. According to Sachs et al. (16) a quarter of the chromosome aberrations formed through the pairwise interaction process are lethal. Possible aberrations are shown in FIG. 2. It takes two DSB to make a chromosome aberration, and about half of them are lethal. Those two factors combined, led to γ equal to 0.25.

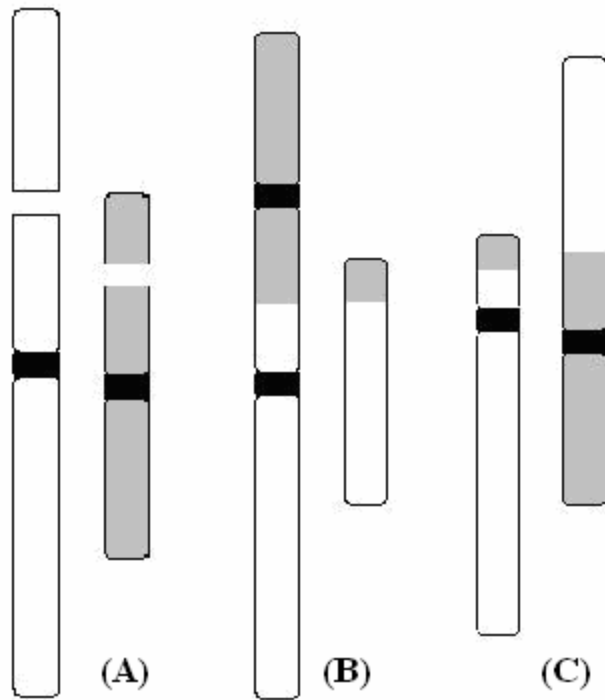


FIG. 2. Example of a chromosome aberration, caused by two DSBs. (A) Two chromatids undergoing DSBs. (B) Dicentric aberration. (C) Translocation aberration.

In addition, only NHEJ could lead to the wide spectra of chromosome aberrations found experimentally (15). Other factors such as chromatin architecture and proximity effects influence the spectra of chromosome aberrations (19). Histones act as natural scavengers for radiation-induced free radicals. Also, chromatin folding and the high degree of compactness of chromatin fiber play a role as protector against ionizing radiation, as it reduces accessibility of free radicals to DNA. The more the chromatin is open, the higher the yield of DSB. According to Radulescu et al. (20) chromatin structure is responsible for the majority of non-randomly distributed DSB induced by high LET radiation. In addition, the increased complexity of damage in the vicinity of high LET DSBs may influence repair times. The presence of many broken ends contributes to the misrejoining, through NHEJ, thus increasing the effective range of interaction and chromosome aberration. Therefore, LET is a parameter to be considered.

Dose rate is also a main parameter when considering the surviving fraction. A radiation dose split into two fractions separated in time increases in cell survival because damage repair happens during the protracted exposure. The longer the protracted exposure is, the more cells survive. As the dose rate is reduced, the slope of the survival curve becomes shallower. Depending on the radiation of interest, the pattern of the DSB deposition in time can be considered either in a deterministic or a stochastic way and these models differ in temporal DSB formation. In the rest of this section we describe the stochastic and non-stochastic nature of DSB deposition. FIG. 3 is a summary of RMR model pathways described above.

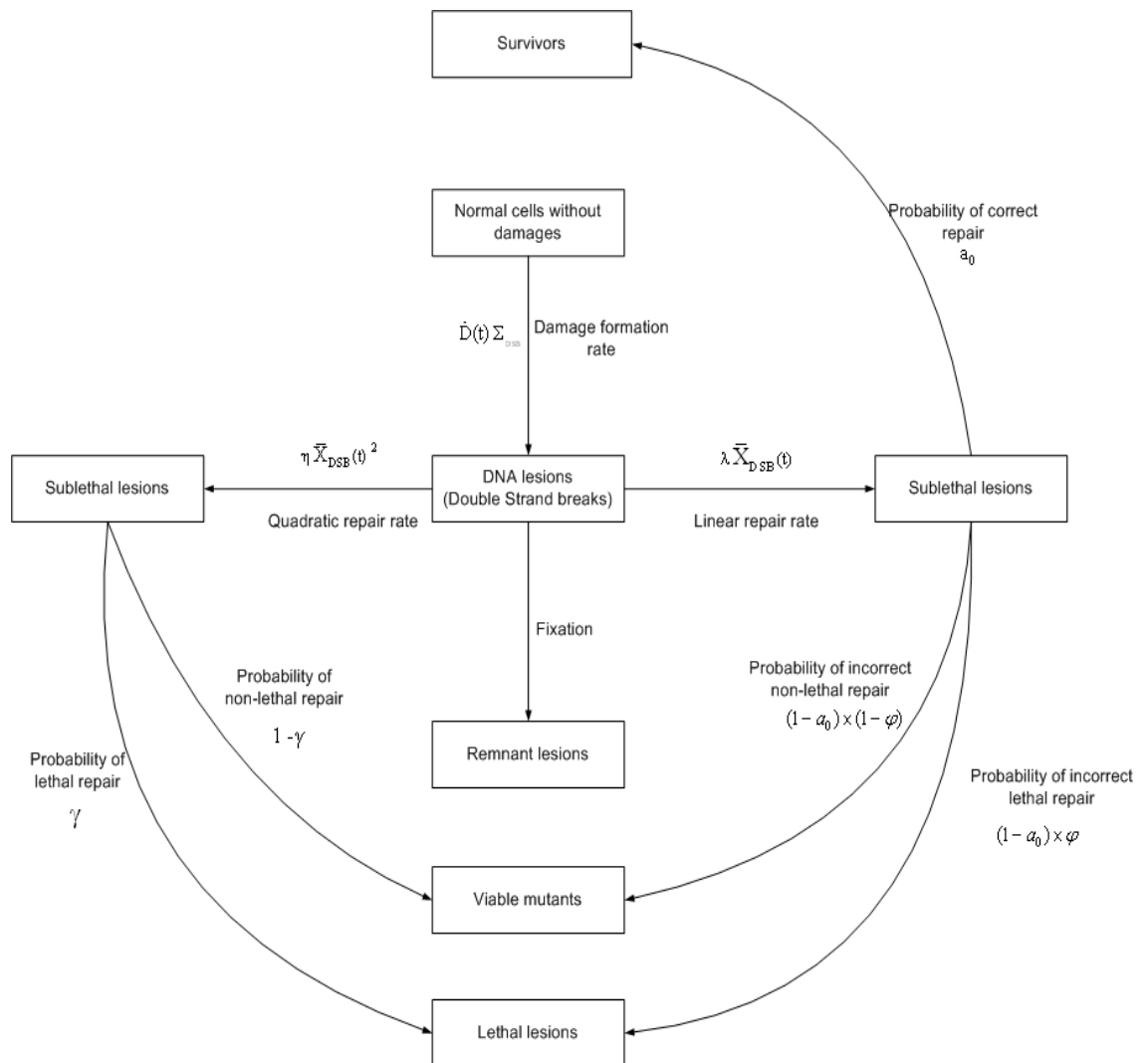


FIG. 3. Summary of the RMR model. An important feature of the RMR model is that it considers several endpoints, linear repair, linear misrepair, quadratic repair, quadratic misrepair, and fixation.

General procedure

A code for implementing the RMR model has been developed in Fortran 90 on a Microsoft Windows workstation.

After choosing a dose, D , a dose rate DR , and a set of radiobiological parameters defined in Eq. (2-3), we assume that cells are continuously irradiated during a time t_d , as the irradiation duration, Eq. (5), and t_d is divided into smaller sub-steps.

$$\text{Irradiation time} = t_d = \frac{\text{Dose}}{\text{Dose-rate}} \quad (5)$$

The key criterion for this approach to work is that the size of each of these sub-steps (Δt) must be much smaller than τ , (e.g., $\Delta t = 0.01 \tau$) to model dose rate effects correctly. As explained before we can think of the expected DSB repair half-time, τ , as the expected amount of time required for a cell to remove (repair or misrepair) half of the DSBs initially produced, as shown in Eq. (4). Next we define how many DSB the cell suffers during each time sub-step. All the DSB deposited are distributed over the whole irradiation period. The pattern of DSB deposition in time depends on whether we consider the problem deterministic or stochastic. We describe both ways later in this section.

There are two cases:

(a) if $t < t_d$, add the number of DSB created during the previous time sub-step. Then integrate Eq. (2-3) from t to $t + \Delta t$, and calculate $X_{dsb}(t + \Delta t)$. $X_{dsb}(t)$ then increases stepwise by the amount defined for that specific sub-step, and $t = t + \Delta t$. One proceeds recursively until $t > t_d$.

(b) if $t > t_d$, we integrate Eq. (2-3) from time sub-step to sub-step until we reach a time cutoff value, with the rate of damage formation set to zero. Also when the cutoff value is reached (usually about a hundred hours) the remaining unrepaired lesions are considered lethal, and added to the total number of lesions. For stochastic models the entire procedure is then repeated for 1000 or more cells and the surviving fraction is computed by taking the average indicated in Eq. (6):

$$S(t) = e^{-L(t)} \quad (6)$$

It is important to note that the differential equation system represented in Eq. (2-3) is integrated using the Visual Numeric's (<http://www.vni.com>) IMSL[®] DIVPAG routine. The IMSL[®] STAT/LIBRARY is a collection of FORTRAN subroutines and

functions useful in research and statistical analysis. This routine uses Gear's backward differentiation algorithm for systems of stiff differential equations.

Deterministic RMR model

Mathematical and computational implementation

The distribution of the number of particle tracks through a cell is well approximated by a Poisson distribution (21). For low LET radiation, the probability one track will make more than one DSB is small (16), and the distribution of the number of DSB per cell should also be well approximated by a Poisson distribution with a mean, \bar{x}_{DSB} , equal to:

$$\bar{x}_{\text{DSB}} = \Sigma_{\text{DSB}} \times D \quad (7)$$

where D is the dose absorbed by a cell, expressed in Gray, and Σ_{DSB} is the number of DSB created per Gray per cell. As described above, the deterministic RMR model uses averaged values. Therefore for the “lesions creation” term, the deterministic model uses \bar{x}_{DSB} , the mean number of DSB created. The surviving fraction S(t) at time t, and the number of lethal damage events created during a short interval, dt, is given by the following expression:

$$\frac{dS(t)}{dt} = - \frac{d\bar{L}(t)}{dt} S(t), S(0)=1 \quad \therefore \quad S(t) = e^{-\bar{L}(t)} \quad (8)$$

To implement the deterministic RMR model, we considered the mean number of DSB, \bar{x}_{DSB} , for one cell. We average the total number of DSB over the whole irradiation period so that an equal number of DSB are created during each sub-step, as described in FIG. 4. In the deterministic model the number of DSB is treated as a real number.

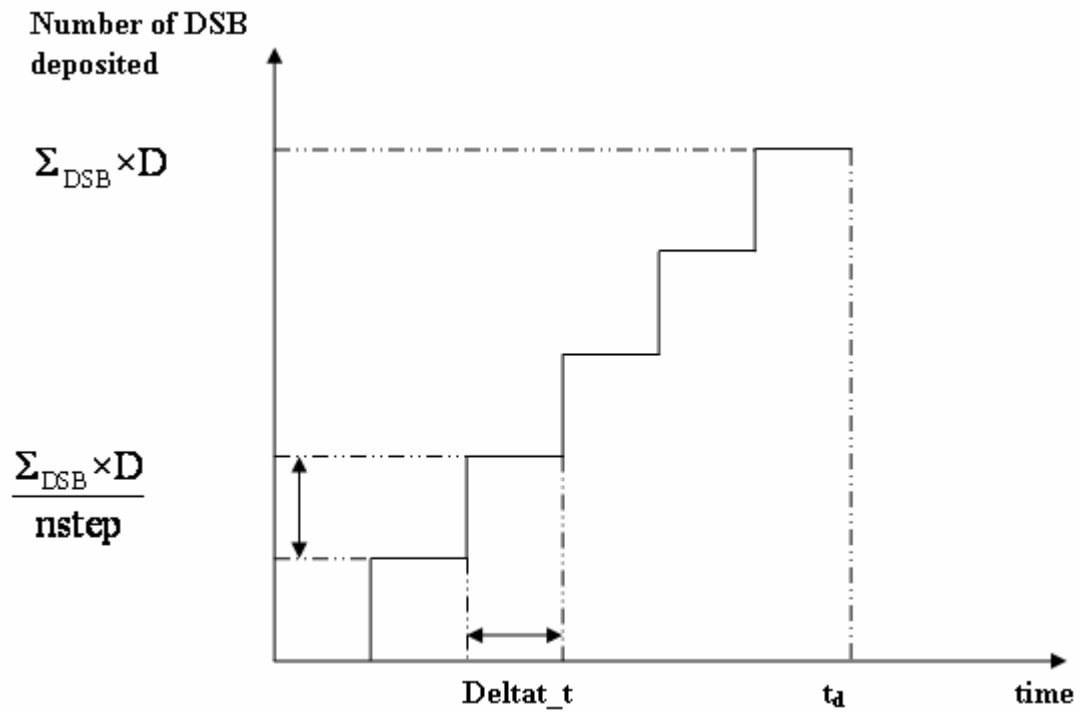


FIG. 4. Pattern of the DSB deposition in time for the deterministic model, with $nstep = t_d / \Delta t$.

Once the deterministic RMR model was developed we need to get the input parameters described in Eqs. (2,3) λ , η , ϕ , a_0 , and γ . We used the VC software to calculate this input.

The Virtual Cell (VC) radiobiology software

The Virtual Cell (VC) software arose from efforts to construct a useful and biologically plausible system of models to simulate early physical, chemical, and biological events and processes involved in the pathogenesis and treatment of cancer. The main biological endpoints of interest in the VC are cell death and neoplastic transformation. The VC also provides information about the formation and repair of DNA damage and some information about chromosome aberration yields, the induction of genomic instability, cell cycle kinetics, and the probability of tumor eradication following radiation therapy. The principal investigator of the Virtual Cell software (<http://rh.healthsciences.purdue.edu/vc/index.html>) development effort is Dr. R.D. Stewart.

The VC software simulates the response of a group of cells following exposure to low or high LET radiation. The software has been specifically designed for use in modeling biological effects following exposure to arbitrary, time-varying radiation levels, e.g., a single dose of radiation delivered at several different dose rates, split-dose exposures, exponentially decreasing dose rates near a radioactive particulate or brachytherapy seeds, and multi-fraction exposure scenarios such as those used in radiation therapy. Output from the VC program includes information on double-strand break (DSB) rejoining kinetics, the yield of lethal and non-lethal mutations by mechanism of action (e.g., fixation, linear misrepair, or binary misrepair, etc.), the genome instability and oncogenic (neoplastic) transformation, and the cell killing.

The collection of models used in the current version of the VC computer program do not explicitly account for many known proliferation-related phenomena, such as cell-cycle blocking or variations in radiosensitivity during the cell cycle. Care should be exercised when using the VC application to analyze radiation effects in proliferating or mixed quiescent/proliferating cell populations. The VC software is best suited to the analysis and prediction of effects in a relatively homogeneous population of quiescent (non-dividing) cells. However, VC models should work reasonably well when the

duration of the exposure is short compared to the duration of the cell cycle. A typically mammalian cell division time is on the order of 10 to 20 h.

Database of radiobiological parameters

The radiation response of a collection of cells is determined by a series of parameters that characterize key molecular and cellular processes. The Virtual Cell automatically provides reasonable default values for all model inputs, and also performs calibration of the model using survival experimental data.

The Virtual Cell (VC) has been designed so that the biological responses to ionizing radiation can be estimated for arbitrary time-varying radiation levels. In the VC, the properties of a time varying radiation field are characterized by the instantaneous absorbed dose rate (Gy/h) as a function of time. This instantaneous dose rate function is termed an exposure scenario. For example external beam radiation treatment (EBRT) or Brachytherapy treatment (BT) can be simulated. Many other types of exposure scenarios are encountered in laboratory experiments, radiation therapy, and certain workplace and environmental settings. To get the input parameters for the RMR model, VC input files describe the radiation exposure scenario, the dose rate and the surviving fraction resulting from the corresponding absorbed dose. Characterizing parameters of molecular and cellular processes, described in the previous section, are then obtained.

VC calibration module also performs Linear Quadratic (LQ) model calculation. The LQ formalism is the most common model used to predict the cell killing effect of radiation. LQ formalism is attractive because it has minimum number of adjustable parameters needed while explaining trends in cells survival as function of dose and dose rate with acceptable accuracy. LQ formalism (22,23) expresses the surviving fraction in terms of a damage coefficient α for lethal lesions made by one-track action, a damage formation coefficient β for lethal lesions made by two track action, and a repair rate λ similar to the first order repair rate described for the RMR model. LQ model is implemented as follows, where S is the surviving fraction:

$$\ln(S) = -\alpha D - \beta G D^2 \quad (9)$$

where G is the generalized Lea-Catchside dose-protraction factor:

$$G = \left(\frac{2}{D^2} \right) \int_{-\infty}^{\infty} \dot{D}(t) dt \int_{-\infty}^t e^{-\lambda(t-t')} \dot{D}(t') dt' \quad (10)$$

The LQ model is widely used in clinical applications and has been discussed extensively in the literature (1,16). From LQ formalism, the α/β ratio is often used to characterize the response of a type of cell to dose fractionation (24). In Eq. (9) α is dose-protraction independent term, while β , the quadratic term in dose, is modified by protraction effects through G the generalized Lea-Catchside dose-protraction factor.

The α/β ratio is a measure of the response of the system to changes in protraction (24). A small value of α/β , in which $\alpha \ll \beta$ would imply a large sensitivity to changes in dose fractionation, while a large value of α/β would imply a small sensitivity to changes in fractionation. Consequently the α/β ratio is a key determinant of fractionation sensitivity of the type of cell that we study.

To perform our calculation we searched the literature presenting survival data. Out of concern for covering the entire range of radiosensitivity parameters expected in mammalian cells we selected cells with small and large alpha/beta ratios, fast and slow repair half-times, and fast and slow quadratic repair. We also choose datasets for low and high LET radiation. These are reported in the Table I. Cell lines are mostly human carcinoma cells, prostate and epithelial larynx tumors, and also normal human fibroblasts cells.

From Eqs. (2,3) we see that VC software predicts the same amount of cell killing regardless of the value of a_0 , as long as the product $(1-a_0)\phi$ remains the same. Since only this product is important, developers of the VC software decided to simplify the

parameterization (i.e. $a_0=0$). So the parameter ϕ , in Table I, really represents the product $(1 - a_0)\phi$.

Table I RMR parameters for all types of cells used in the calculation.

Cell line	α (Gy ⁻¹)	β (Gy ⁻²)	α/β (Gy)	λ (h ⁻¹)	η (h ⁻¹)	ϕ	Reference
A549	1.56E-01	5.27E-02	2.96E+00	1.45E+01	1.00E-02	6.24E-03	(25)
AG01522	1.88E-01	4.16E-02	4.51E+00	8.01E-01	4.40E-04	7.50E-03	(26)
DU145	2.69E-01	5.04E-02	5.32E+00	9.30E-02	1.27E-05	4.88E-03	(27)
HX118	3.14E-01	3.92E-02	8.02E+00	2.46E+00	1.30E-03	1.26E-02	(28)
Hela	2.43E-01	2.49E-02	9.78E+00	6.53E-01	2.16E-04	9.73E-03	(29)
M10	8.81E-01	3.74E-03	2.36E+02	3.39E-01	1.89E-05	3.52E-02	(30)
SQ20B	1.79E-01	1.07E-02	1.67E+01	3.50E-01	4.95E-05	7.17E-03	(30)

The VC software is a deterministic model. Therefore the calculated RMR parameters are best when they are used with a deterministic RMR model. However we use these same parameters as an input of the SRM. The VC software is the best tool available to achieve RMR model this task. There is no equivalent stochastic tool available at this time.

Stochastic RMR model

Microdosimetric considerations

Originally formulated in terms of the average of numbers of unrepaired and lethally mis-repaired DSBs in a cell, as described above, deterministic RMR model uses

two statistical approximations. First, it neglects the effects of statistical fluctuations in the number of DSB in a cell. Second, it assumes that the number of unrepaired and lethally misrepaired DSB has a Poisson distribution (2,3,16). As particle LET increases, the chance a track will create more than one DSB in the same cell increases. This intra-track clustering of DNA damage can produce non-Poisson distributed DNA damages. That is, the distribution of DNA damage among identically irradiated cells is the result of a so-called CPP (21).

A CPP is a distribution arising from two mixed Poisson processes. It is a process of independent events, or particle tracks, of varying magnitude, or energy deposition.

Models using microdosimetry have been proposed to better account for LET effects and, in particular, deviations from Poisson distributions of DNA damage (31). In a small site such as a cell nucleus, the specific energy per event, z_1 , is taken as follows:

$$z_1 = \frac{\varepsilon}{m} \quad (11)$$

where m is the mass of the site, and ε is the energy imparted to a volume of interest by an energy deposition event. The single event specific energy, z_1 is the stochastic equivalent of absorbed dose and is expressed in joules per kilogram or Gray.

LET, or lineal energy (its microscopic equivalent) is usually used to describe the energy deposition within a site of interest. The lineal energy, y , is the energy deposited per unit length, and is defined as the quotient of ε by \bar{l} , where ε is the energy imparted to a volume of interest by an energy deposition event, and where \bar{l} is the mean chord length in that volume:

$$y = \frac{\varepsilon}{\bar{l}} \quad (12)$$

The lineal energy is expressed in joules per meter, or also may be expressed in keV per micrometer a more convenient unit.

In a single event the relationship between z_1 and y is (33):

$$z_1 = \frac{\varepsilon}{m} = \frac{\frac{2}{3}d \times y}{\rho S} \quad (13)$$

According to a theorem by Cauchy, the mean chord length in a convex site is given by $(4V)/S$, where V and S are respectively, the volume and the surface of the site. In the typical case of spherical sites $S=4\pi r^2$ and so we have:

$$z_1 = \frac{y}{4\pi r^2} \quad (14)$$

In most applications of microdosimetry ρ is taken to 1g/cm^3 , z is given in the units of gray, y is expressed in $(\text{keV}/\mu\text{m})^2$ and r is μm . With these units we have:

$$z_1 = \frac{0.204y}{(2r)^2} \quad (15)$$

In our context the volume of interest is the cell nucleus that has a diameter of about $10\mu\text{m}$. Finally z is expressed as follows:

$$z_1 = 20.4y \quad (16)$$

Instead of considering an average value over a site, probability distributions are considered.

According to Rossi and Zaider (32) the term “ionizing radiation” needs to be based on the concept of relevant energy transfer point. Kellerer also calls them events. According to IRCU #36 (33) events are statistically independent. We often consider

independent charged particles traversing the site of interest, the cell nucleus, in straight paths randomly distributed through the cell, as shown in FIG. 5 A. An event in this context refers to all the ionizations caused by one primary radiation particle and its secondaries within the nucleus.

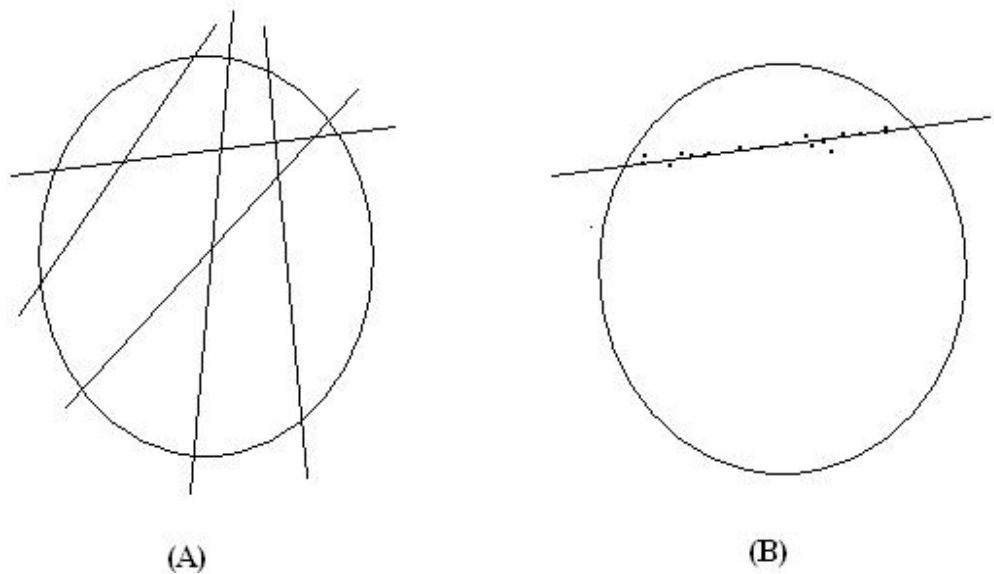


FIG. 5. CPP for the energy deposition inside a site at a specified dose. On (A) several tracks or events are going through the cell. Dots on (B) represent ionizations.

The number of particle tracks, or events, through a cell is well approximated by a Poisson distribution (21). In addition the number of DSB created along a particle track is also well approximated by a Poisson distribution, as shown in FIG. 5B (16). \bar{z}_1 is the mean specific energy per event. The expected number of events during the time interval corresponding to a specified absorbed dose D is:

$$\bar{v} = \frac{D}{\bar{z}_1} \quad (17)$$

Accordingly, the event frequency per unit absorbed dose is :

$$\frac{1}{\bar{z}_1} \quad (18)$$

Once the number of events per cell is known, the number of DSB per event is then computed. The mean number of DSB per event is:

$$\bar{x}_{\text{DSB}} = \Sigma_{\text{DSB}} \times \bar{z}_1 \quad (19)$$

where Σ_{DSB} is the number of DSB created per Gray per cell. Values from the literature suggest Σ_{DSB} should be about 25 DSB created per Gray per cell (18). To get the number of DSB created per track, the first possibility is to consider the LET, and so the specific energy z , as constant values. This assumption is adequate in case of track segment experiments where changes in energy deposition along the particle track are negligible. The other possibility is to take into account the variation of energy deposited along the particle track. To do so we considered two options.

The first option is to apply chord length distribution $f(l)$, expressed in Eq. (20) and described in FIG. 6, to account for changes in energy deposited along the tracks.

$$f(l) = \frac{2l}{d^2} \quad (20)$$

where l is the actual chord length and d the diameter site. We can express the specific energy deposited in terms of the chord length (21):

$$z(l) = 0.306 \frac{1}{\rho} \frac{y}{(d)^3} \quad (21)$$

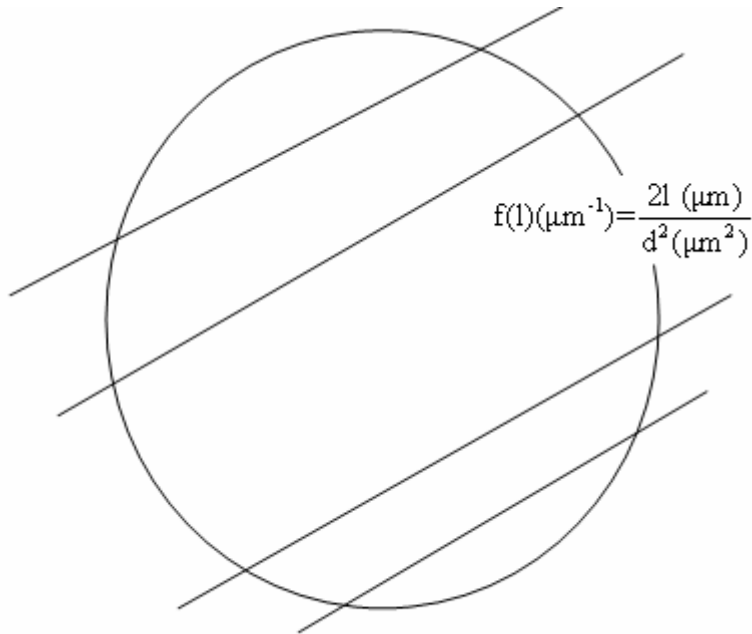


FIG. 6. Diagram illustrating the variation in the chord length distribution within the site of interest. In a sphere of diameter d the chord length distribution, $f(l)$ is triangular.

Because the simple direct expression for the chord length distribution is easy to integrate, the implementation in a Monte Carlo code is straightforward. Other stochastic factors may be important in the microdosimetric spectrum. For example energy loss straggling, Fano fluctuations, i.e., the number of ions produced per unit energy deposition (33), and secondary particles effects may play a role. That is why we looked at a second method.

To better account for these effects we formulated a second Monte Carlo code that used specific energy distributions. The goal is to take into consideration the random processes occurring in the site of interest such as formation of crossers, stoppers, insiders, and starters. They are represented in FIG. 7.

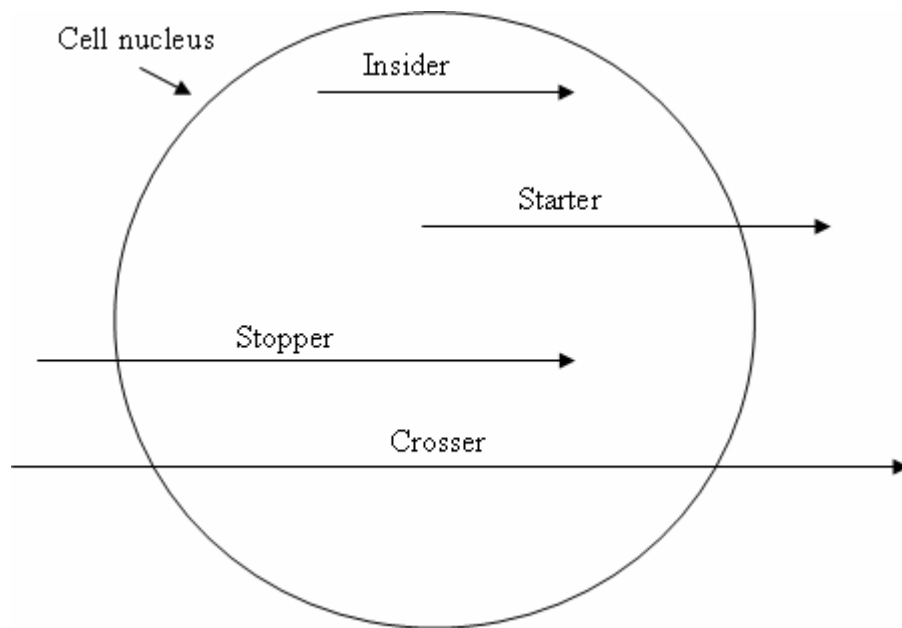


FIG. 7. Diagram describing four classes of tracks: crossers, particles going all the way through the cell nucleus; stoppers, particles stopping inside the cell nucleus; starters, secondary particles initiated inside the cell nucleus and leaving the cell nucleus; and insiders, secondary particles initiated and stopping inside the cell nucleus.

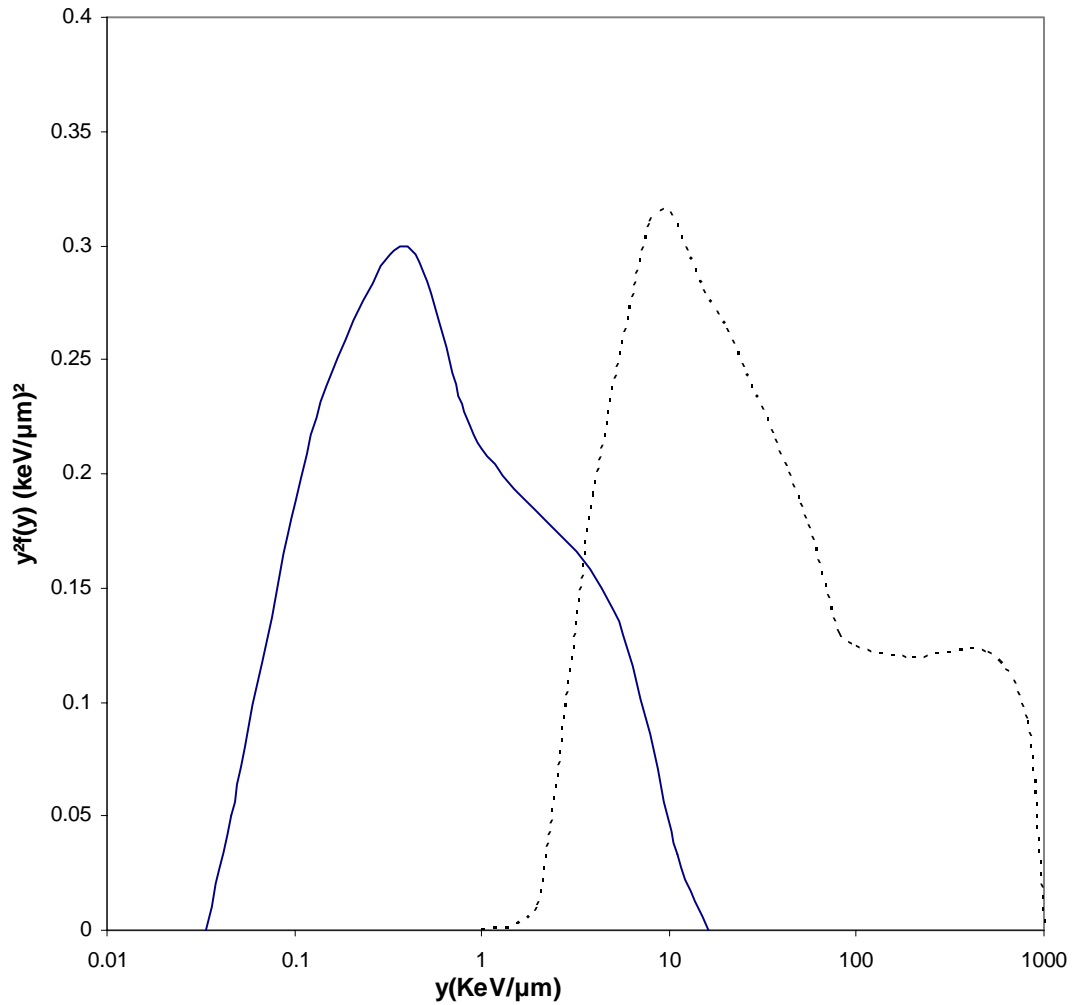


FIG. 8. Lineal energy distribution for a spherical tissue region of one micrometer in diameter for (—) ^{60}Co gamma radiation, and for (--) 15MeV neutrons.

FIG. 8 shows typical specific energy distributions from ICRU #36 for ^{60}Co gamma radiation, and for 15MeV neutrons.

First, we sample the lineal energy from the distribution, and then we can calculate the specific energy with Eq. (13). Once we calculate the specific energy deposited we compute the number of DSB deposited.

We computed these distributions and built a Monte Carlo code out of it. Details of the computational implementation are described next.

Finally, the total number of DSBs deposited is computed for all tracks. Then we consider the pattern of damage deposition in time. According to Sachs et al. (4) the specific energy impartation occurs in bursts. How we model this distribution of DSB over the time is explained below.

Computational implementation

To compute the so-called CPP described above, we used a Monte Carlo method.

First, we defined the number of tracks going through a cell by calling the RNPOI sub-routine, the IMSL[®] routine RNPOI gives a random number out of a Poisson distribution defined by its mean. The mean number of tracks per cell being is defined in Eq. (19). Then for each track we compute the number of DSB deposited along a track. As explained above we used three different models to evaluate the energy deposited per track: 1) CPP with LET constant, 2) CPP using chord length distribution, 3) CPP using specific energy distribution.

1) CPP with LET constant

We compute the DSB created within a cell nucleus according to this algorithm:

(a) we compute the number of tracks going through the cell with a Poisson process with a mean defined in Eq. (17).

(b) for each track we compute the number of DSB created with Eq. (19). The sum of all the DSB created within a nucleus is then computed.

2) CPP using chord length distribution

We compute the DSB created within a cell nucleus according to this algorithm:

(a) we compute the number of tracks going through the cell with a Poisson process with a mean defined in Eq. (17).

(b) the chord length distribution defined in Eq. (20) has a mathematical form easy to integrate. Then using Monte Carlo technique we generated chord length with equation (22).

$$l=d\sqrt{\xi} \quad (22)$$

where d is the site's diameter and ξ is a random number ranging from zero to one. Then we calculate the specific energy with Eq. (21) and get the number of DSB. We repeat this process for each track.

3) CPP using specific energy distribution

(a) we generate histograms from specific energy distributions shown in FIG.8.

(b) we use rejection technique to generate specific energy. If the probability range from zero to h , and the lineal energy values range from y_1 to y_2 , we generate the probability p of having a lineal energy equal to y according to Eq. (23-24).

$$p = \xi_1 (y_2 - y_1) + y_1 \quad (23)$$

$$y = \xi_2 h \quad (24)$$

where ξ_1 and ξ_2 are two random numbers ranging from zero to one. If p is greater than the probability of having the lineal energy value equal to y , then we reject it, and repeat the process. We generate this algorithm for each track, so that we compute the energy deposited for each of them.

c) Finally we randomly distribute the radiation events over the irradiation period, so that the time pattern of DSB deposition stays a stochastic process.

RESULTS AND DISCUSSION

Test of the initial DSB distribution

We simulated the damage formation of DSBs using various CPP. To test the hypothesis that the Poisson distribution, with a mean equal to $D \times \Sigma_{\text{DSB}}$ provides an adequate representation of the initial distribution of DSBs as function of dose, D , and mean specific energy, \bar{z}_1 . Specific energy is directly related to the LET or particle lineal energy as seen in Eq. (16). In Table II are reported results comparing Poisson distributions associated moments with the exact solutions of the associated moments generated using Monte Carlo methods and CPP.

There is a good agreement between the mean values of the Monte Carlo generated distributions with constant LET and the first moment of the Poisson distribution, but the standard deviations agree less well. For low values of the specific energy, $\bar{z}_1 = 0.001 \text{ Gy}$, (low LET), and any dose, Poisson distribution provide adequate representation of the initial distribution of DSB; the mean values and standard deviation of the solutions generated using Monte Carlo methods with constant LET gives very good approximation of the means of the Poisson distribution. On the contrary for high specific energy values, $\bar{z}_1 = 0.1 \text{ Gy}$, mean values generated using Monte Carlo methods gives good approximation of the associated moments of the Poisson distribution, but the standard deviations generated using Monte Carlo methods are almost twice as large as the standard deviation of the associated Poisson distribution.

Besides, according to chi-square tests probability shown in Table II, it is likely that for low specific energy that the initial distribution of DSB will be Poisson distributed as shown in the same table. On the contrary, for high specific energy value, the initial distribution of DSB diverges from Poisson distribution.

Table II Comparison of the Poisson distribution associated moments with the exact solutions of the associated moments generated using Monte Carlo method with CPP, CPP considering chord length distribution, and CPP considering specific energy distribution.

Simulation characteristics	Poisson distributions associated moments		Solutions generated using Monte Carlo methods		Probability of χ^2 test (comparing solutions generated using Monte Carlo methods and Poisson distribution)	Solutions generated using Monte Carlo methods with actual chord length distribution		Solutions generated using Monte Carlo methods with specific energy distribution	
	Mean value	Standard deviation	Mean value	Standard deviation		Mean value	Standard deviation	Mean value	Standard deviation
z1b=0.001Gy D=1Gy	25	5	24.9696	5.07784	0.41	27.2652	7.23698	28.77401	16.74982
z1b=0.1Gy D=1Gy	25	5	25.0819	9.32098	less than 0.01	25.98745	12.74987	30.74568	27.52036

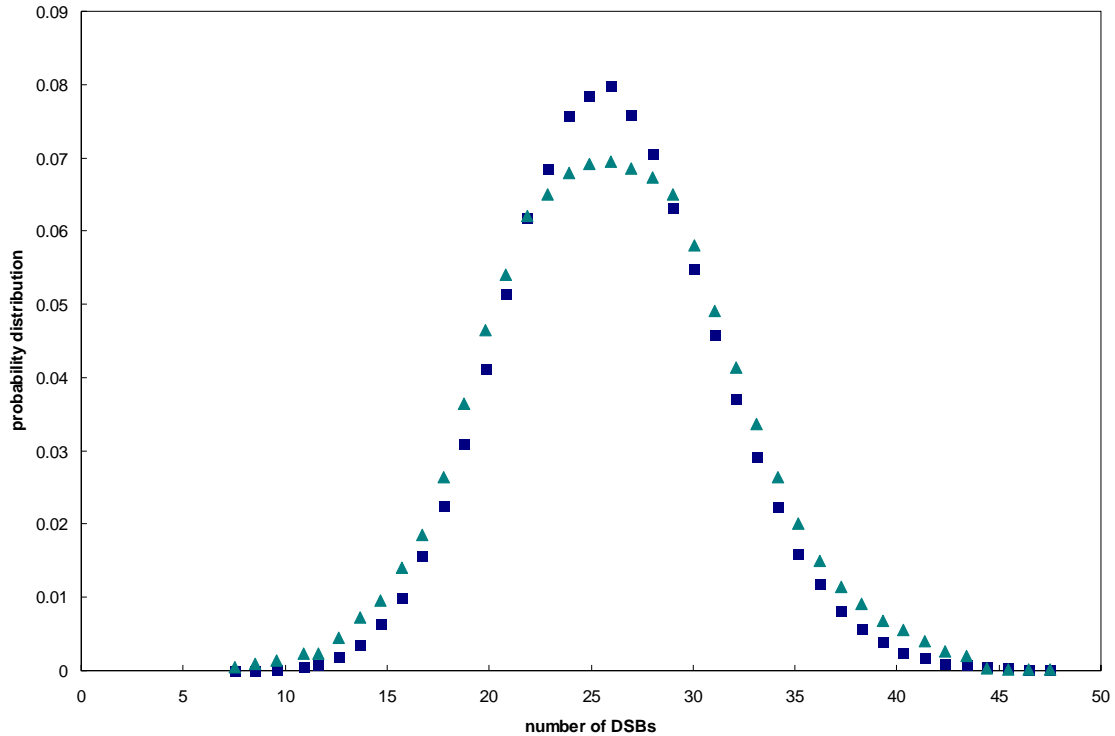


FIG. 9. DSBs probability distribution for $\bar{z}_1=0.001\text{Gy}$ and $D=1\text{Gy}$, corresponding to low LET radiation. (■) probability distribution of the number of DSBs predicted with a CPP. (▲) probability distribution of the number of DSBs predicted with a CPP and taking into account the chord length distribution. (■) $\bar{x}=24.9696$, and $\sigma=5.07784$. (▲) $\bar{x}=27.2652$ $\sigma=7.23698$.

For the same dose value, FIG. 9 and FIG. 10 show the change in the shape of the probability distribution curves. Going from high to low specific energy, increases the standard deviation and so widens of the curve. Therefore as LET increases a Poisson distribution does not approximate the probability distribution of DSBs as well as it does for low LET values. Sachs et al. (4,5) and Albright (3) explored the validity of the approximation of the initial distribution of DSBs. Using Markov models, they pointed out as well that Poisson distribution hypothesis is relevant for the initial DSBs distribution at low LET, but not anymore for high LET radiation. We use Monte Carlo

methods to specifically incorporate better stochastic fluctuations in DNA damage formation.

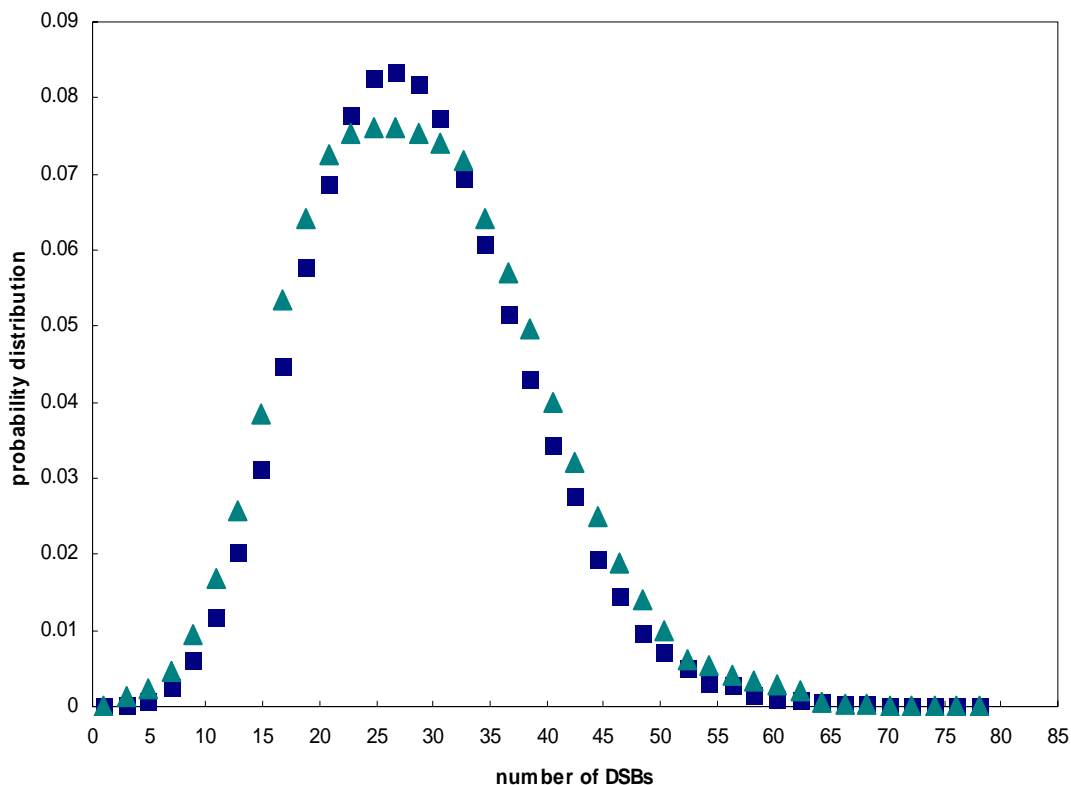


FIG. 10. DSBs probability distribution for $\bar{z}_1=0.1\text{Gy}$ and $D=1\text{Gy}$, corresponding to low LET radiation. (■) probability distribution of the number of DSBs predicted with a CPP, (▲) probability distribution of the number of DSBs predicted with a CPP and taking into account the chord length distribution. (■) $\bar{x}=2.0819$, and $\sigma=9.32098$. (▲) $\bar{x}=25.98745$, and $\sigma=12.74987$.

We repeated the calculation with the CPP and added the variation of the chord length. Knowing the chord length distribution we incorporated it in the Monte Carlo code to account for the variation of energy deposited inside the nucleus. Equation (21) shows the relationship between the specific energy deposited and the chord length. We can observe in the DSB distributions shown in FIG. 9 and FIG. 10 that the spectrum is slightly broader when we consider the variation in the chord length. In addition we

compare the mean and the standard deviation of both distributions with and without the use of the chord length distribution. We can see that both moments are close. First and second moments are reported in Table II.

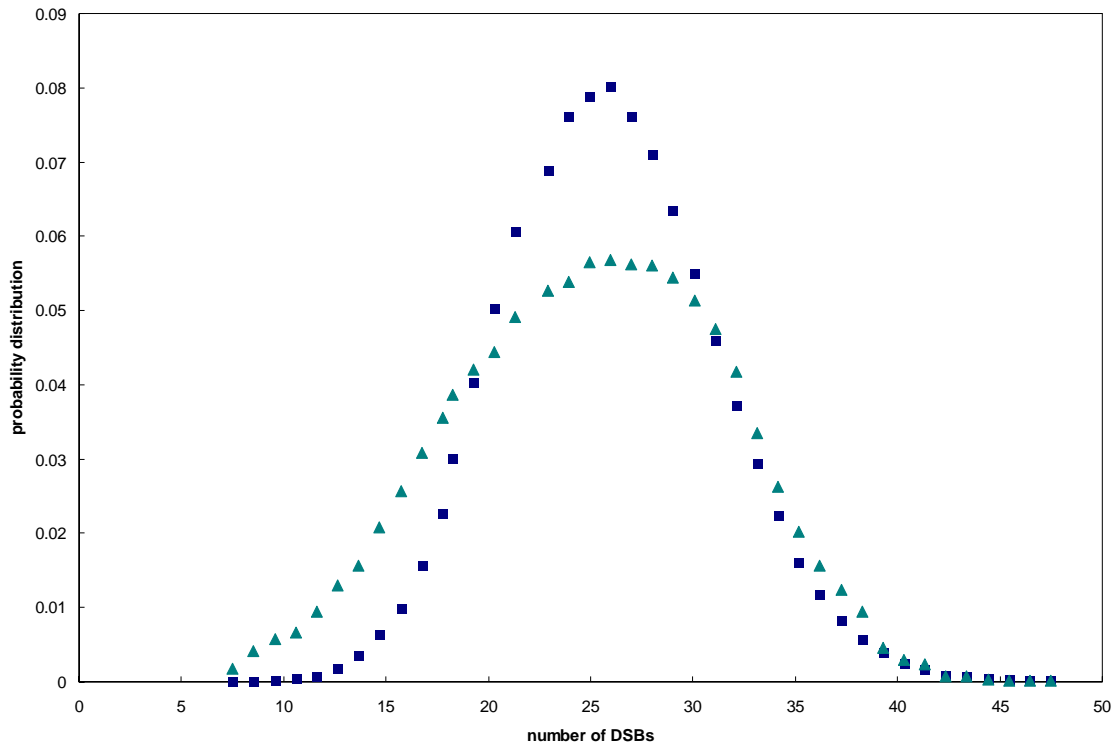


FIG. 11. DSBs probability distribution for low LET radiation and $D=1\text{Gy}$, corresponding to low LET radiation. (■) probability distribution of the number of DSBs predicted with a CPP, (▲) probability distribution of the number of DSBs predicted with a CPP and taking into account the specific distribution. Specific energy distribution is taken from ICRU#36 (33) for Co-60 gamma radiation. (■) $\bar{x}=24.9696$, and $\sigma=5.07784$. (▲) $\bar{x}=28.77401$ $\sigma=16.74982$.

Lastly, we performed survival calculations considering the specific energy distribution from ICRU#36. FIG. 11 shows the DSB distribution using specific energy distribution for low LET radiation (gamma radiation from ^{60}Co) taken from ICRU#36. In FIG.11 we can see that more low levels of DSB occurrence appear. This is due to small amounts of energy deposited by secondary electrons, then making the spectrum broader. Similarly FIG. 11 shows a larger spectrum compare to the Poisson distribution, because of the variation of energy deposition within the cell nucleus.

FIG. 12 shows the DSB distribution using specific energy distribution for higher LET radiation (15 MeV neutrons) taken from ICRU#36. When we take into consideration specific energy distribution from ICRU#36 we observe that DSB distribution diverge from pure Poisson distributions. Typically these differences are due to random processes (energy loss straggling, Fano fluctuations i.e. the number of ions produced per unit energy deposition (33), and secondary particles effects) occurring inside the nucleus.

Also, we can see in FIG. 11 and in FIG. 12 that high levels of DSB occur more often if we consider typical specific energy deposition. This observation will be important when we will consider survival results calculated with CPP using specific energy distribution model.

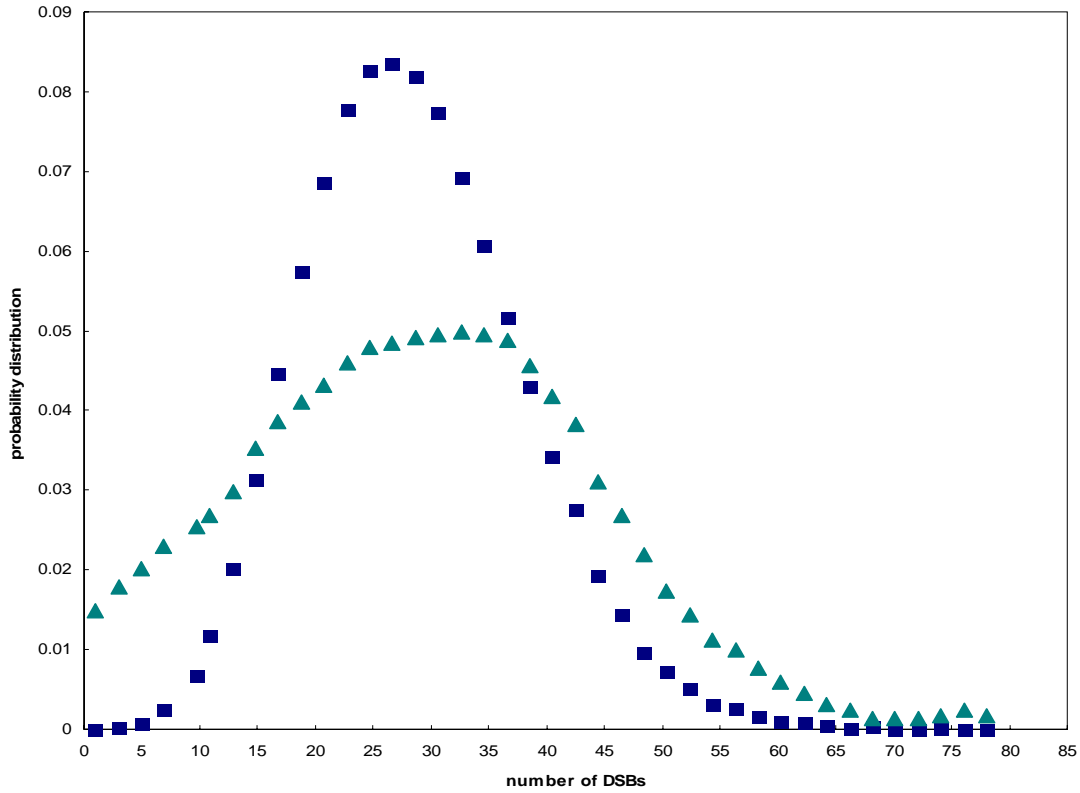


FIG. 12. DSBs probability distribution for high LET radiation and $D=1\text{Gy}$, corresponding to low LET radiation. (■) probability distribution of the number of DSBs predicted with a CPP, (▲) probability distribution of the number of DSBs predicted with a CPP and taking into account the specific distribution. Specific energy distribution is taken from ICRU#36 (33) for 15 MeV neutron. (■) $\bar{x}=24.9696$, and $\sigma=5.07784$. (▲) $\bar{x}=30.74568$ $\sigma=27.52036$.

Analytical verification

We use the CPP to simulate the stochastic aspect of the DNA damage formation and built a Stochastic RMR model (SRM) software to simulate the repair processes and compute the final number of lethal lesions throughout a cell and the surviving fraction of cell population. RMR differential equations, Eqs. (2,3) have trivial analytical solutions for selected problems. This section presents an analytical verification of the SRM software.

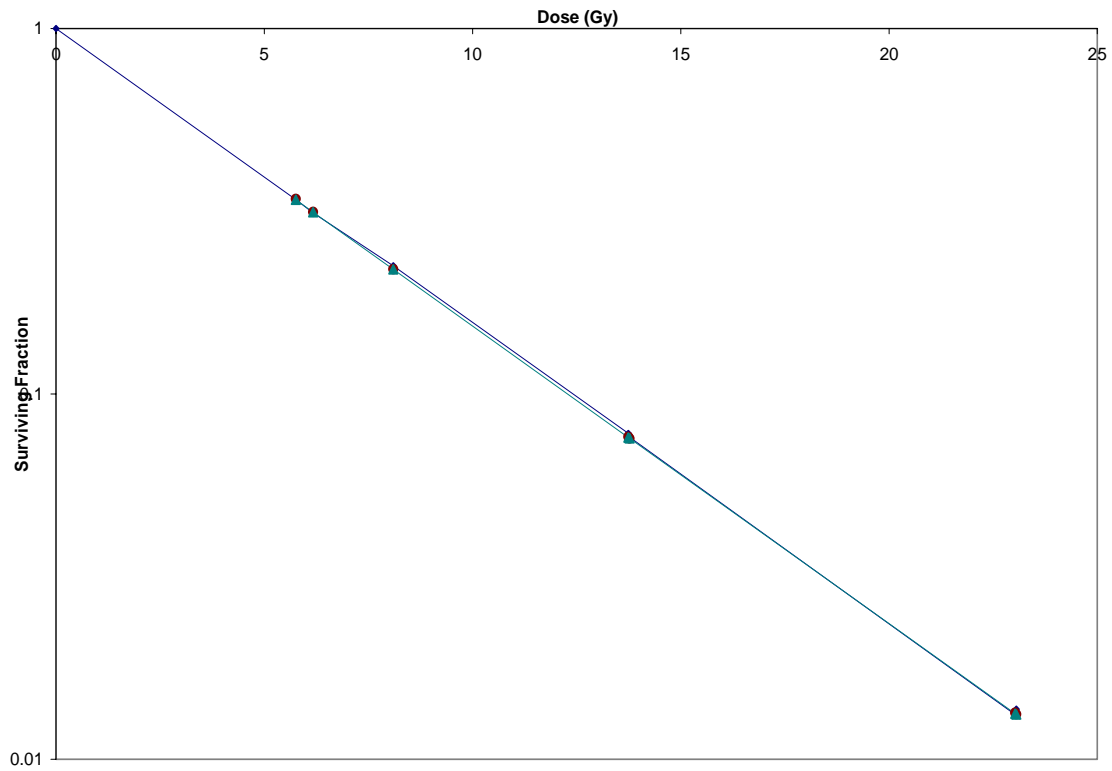


FIG. 13. Comparison of stochastic (●), deterministic (■), and analytical (▲) results for a selected case, i.e. with the binary misrepair term set to zero. Dose rate is equal to 0.34 Gy/h.

Shown in FIGS. 13 and 14 are surviving fraction curves for cell line AG01522 for several dose rates.

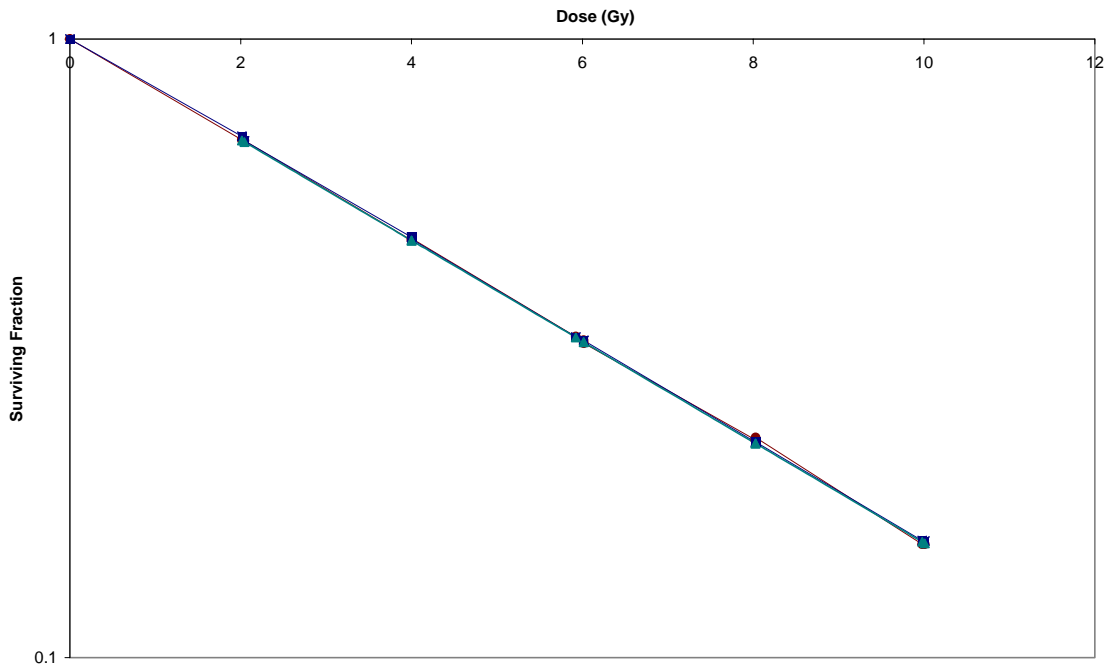


FIG. 14. Comparison of stochastic (●), deterministic (■), and analytical (▲) results for a selected case, i.e. with the binary misrepair term set to zero. Dose rate is equal to 81 Gy/h.

The plots present in abscissa the dose and in ordinate the surviving fraction of a population of 10^4 cells. As in the previous case, the data is collected at different dose rates (from low dose rate of 0.34 Gy/h to high dose rate of 81 Gy/h).

The stochastic, deterministic and analytical results agree within 5% along the different dose and dose rate values. This level of accuracy is sufficient for the purpose of this study. Together with the analytical results, the deterministic results agree results from the SRM software. The SRM software appears to be correctly implemented and verified.

Evaluating the accuracy of SRM software

In this section survival curves obtained with SRM software are compared with measured results from literature, and with deterministic results. Deterministic results are obtained using SRM software switching off the stochastic aspect of damage formation. RMR parameters used in the calculations are the ones identified in Table II. We present a few representative examples to illustrate general features. We distinguish between calculations for low and high LET: low LET simulation with AG01522 type of cells, and high LET simulation with SQ20B type of cells.

Note that all surviving fractions calculated with SRM are given with associated standard error bar to take into account any statistical noise.

In our model we did not consider cell proliferation and cell cycle effects.

Low LET radiation

First we present measured, deterministic, and stochastic survival curves for low dose rates of 0.24Gy/h and 0.71Gy/h shown in FIG. 15. The deterministic results overestimate the surviving fraction compared to stochastic results. We can explain this by noting that, for any fluctuating variable, the average of squares is greater than the square of the average, $\overline{X_{DSB}^2} < \overline{X_{DSB}}^2$ (4), leading to extra cell killing in Eq. (3) of RMR model.

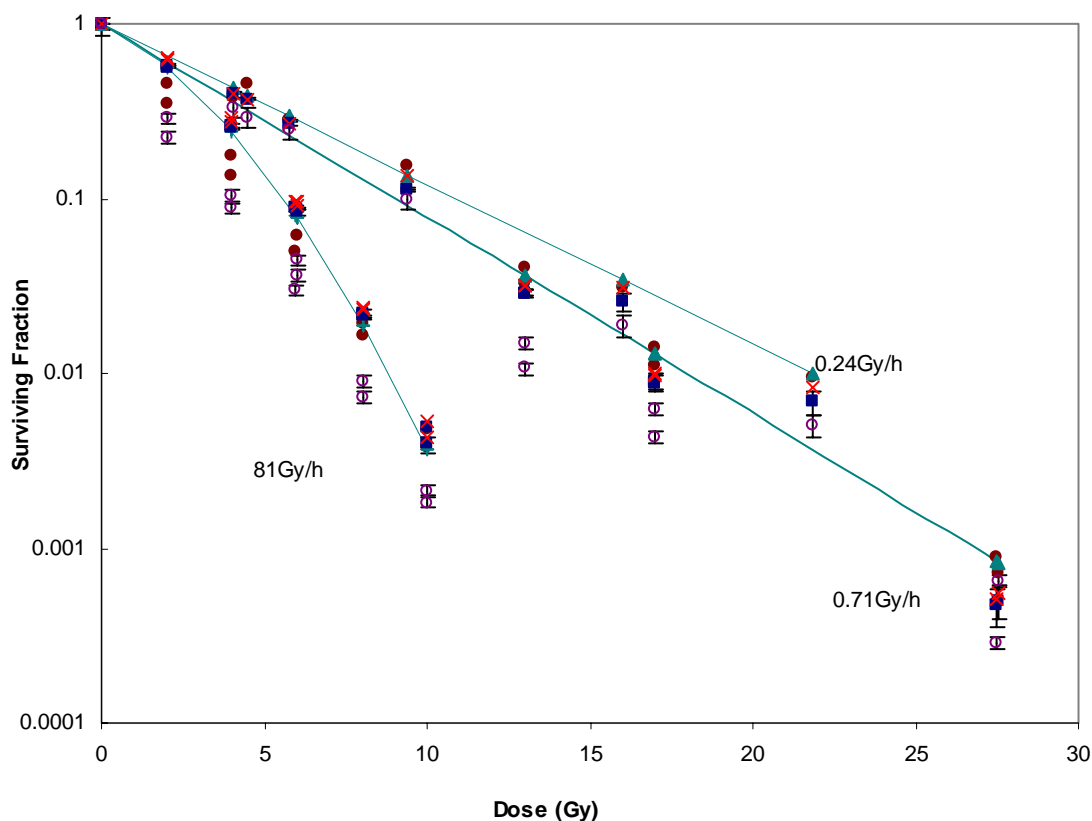


FIG. 15. Comparison of survival results for various low dose rate, 0.24Gy/h and 0.71Gy/h, and high dose rate, 81Gy/h, for low LET radiation, 0.01keV/ μ m, and for cell line AG01522. (●) Surviving fraction measured by experiments. (▲) Surviving fraction predicted by deterministic RMR model. (■) Surviving fraction predicted by stochastic RMR model. (×) Surviving fraction predicted by stochastic RMR model taking into account the chord length distribution. (○) Surviving fraction predicted by stochastic RMR model taking into account the specific energy distribution.

Furthermore, for low dose rates, such as the example presented here, the time of irradiation is long. Deterministic model artificially spreads the creation of DSB uniformly over the irradiation period. Therefore repair and misrepair can almost run their full course between events, distorting the effectiveness of repair in the obtained results. This effect is not encountered using the stochastic approach of damage formation and we can observe the absence of a significant shoulder in the survival curve. This is normal as

continuous low dose rate irradiation may be considered as an infinite number of infinitely small fractions and the survival curve would be expected to have no shoulder (34).

FIG. 15 also shows comparison of measured, deterministic, and stochastic survival curves for high dose rates (81Gy/h). The stochastic RMR model survival curve is non-linear at low doses. We can also observe that stochastic results obtained with CPP and CPP with chord length distribution both lead to extra survival compared to deterministic results. As explained by Sachs (4) the extra survival is primarily because the exponential function is concave upward so that the average of the exponential is greater than the exponential of the average, $\overline{e^{-L(t)}} > e^{-\overline{L(t)}}$, this inequality holds in Eq. (8). Unlike low dose rate survival curves, high dose rate survival curves show a shoulder. At high-dose rate this shoulder is due to the accumulation of sub-lethal damage. However the shoulder is small and the survival curve is steep compared to other type of cells with a smaller α/β ratio. For example when comparing high dose rate survival curve for AG01522 cell line in FIG. 15 to the A549 cell line in FIG. 16 we can see that at high dose rate the shoulder is slightly bigger for A549 survival curves. Because the α/β ratio is somewhat smaller for A549 cell line, 2.9 Gy, compared to 4.5 Gy for AG01522 cell line. More generally we can say that stochastic RMR software reproduces correctly the shoulder observed at high dose rate in experimental as well as deterministic results. The appearance of this shoulder has several explanations. It may have come either from the saturation of repair processes, or from the non-linear production of initial DSB or from interactions of lesions produced by statistically independent tracks. This last reason is the one considered in the RMR model, and stochastic RMR model also follows this feature even when statistical fluctuations are taking into consideration.

Other survival curves for cell lines A549, HeLa, HX118, and M10 are reported in FIG. 16. Cell lines A549, HeLa, and HX118 are given for low LET (^{60}Co gamma radiation). While cell line M10 is given for higher LET (15 MeV neutron).

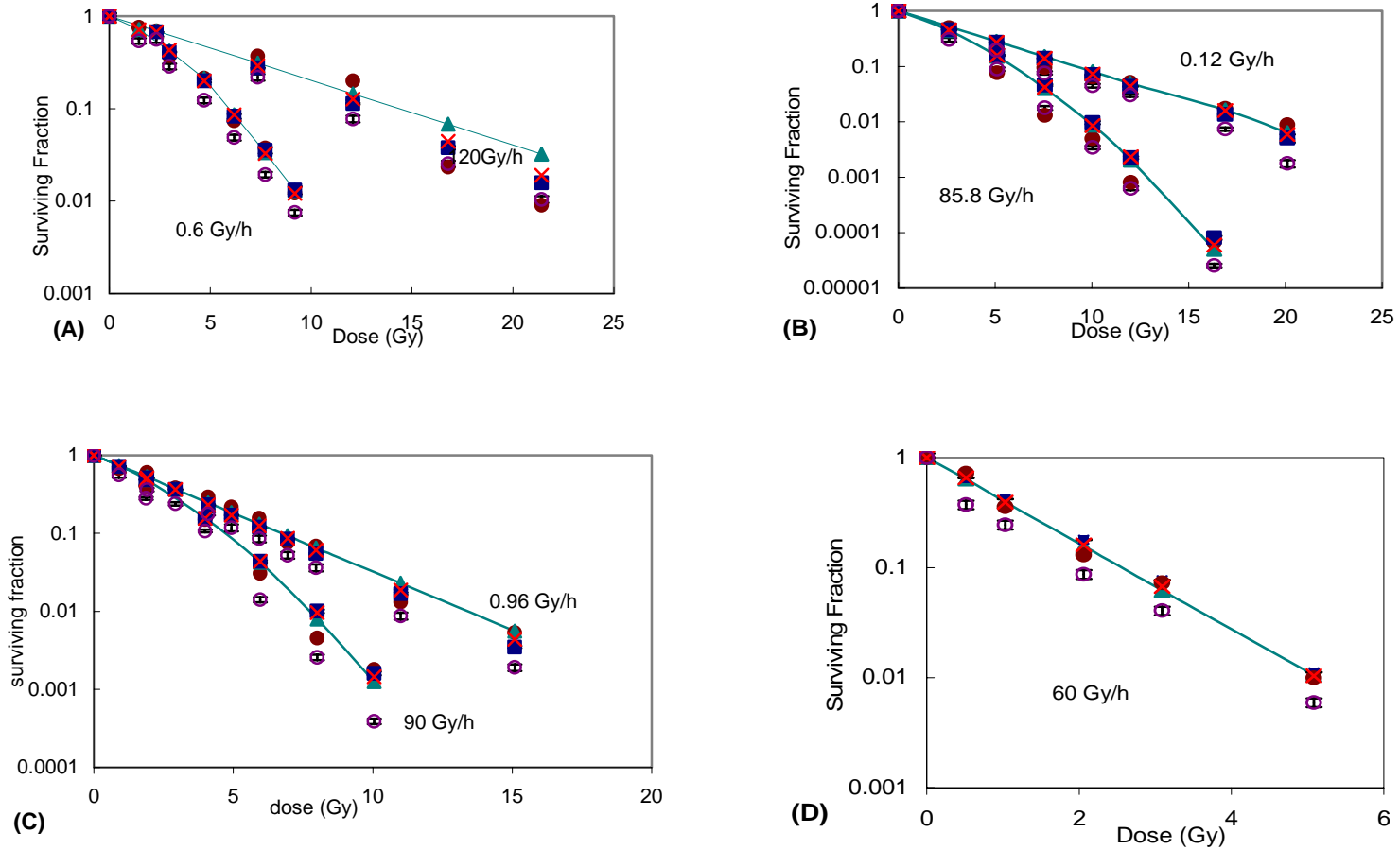


FIG. 16. Comparison of survival results for several cell lines: (A) A549, (B) HeLa, (C) HX118, and (D) M10. (●) Surviving fraction measured by experiments. (▲) Surviving fraction predicted by deterministic RMR model. (■) Surviving fraction predicted by stochastic RMR model. (×) Surviving fraction predicted by stochastic RMR model taking into account the chord length distribution. (○) Surviving fraction predicted by stochastic RMR model taking into account the specific energy distribution.

Finally, we observe in FIG. 15 that survival results using specific energy distribution diverge from the other survival results. More investigation is needed to explain why CPP with specific energy distribution underestimate surviving fraction. A beginning of explanation could be that we are using RMR parameters calculated with a deterministic model, which may be not compatible when using such a stochastic model.

High LET radiation

We present below survival curves for high dose rates and high LET radiation.

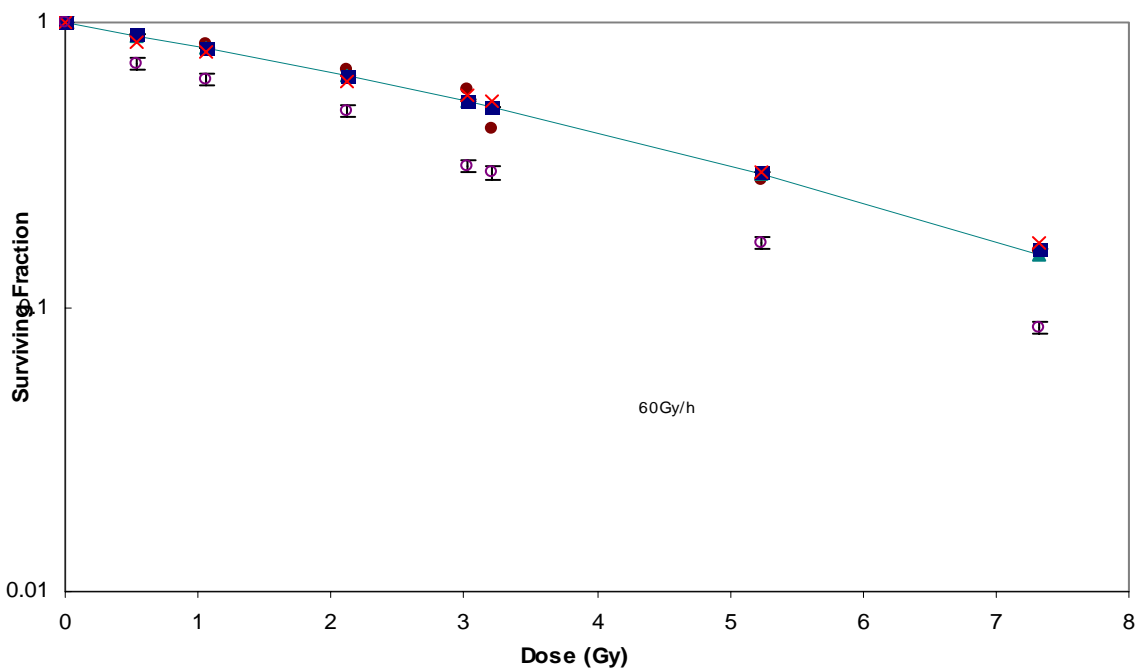


FIG. 17. Comparison of survival results for high LET radiation, and for cell line SQ20B. Results are presented for a dose rate of 81Gy/h and particle LET of 19.8keV/ μm . (●) Surviving fraction predicted by experiments. (▲) Surviving fraction predicted by deterministic RMR model. (■) Surviving fraction predicted by stochastic RMR model. (×) Surviving fraction predicted by stochastic RMR model taking into account the chord length distribution. (○) Surviving fraction predicted by stochastic RMR model taking into account the specific energy distribution.

As would be expected for high LET radiation, the survival curves in FIG. 17 show almost no shoulder. At low doses stochastic and deterministic RMR survival curves agree fairly well, and show the same shoulder at the beginning of the survival curve. As dose increases, both stochastic CPP, and CPP with chord length distribution, and deterministic RMR survival curves asymptotically approach a final curve. We can note a somewhat small discrepancy at high dose, where stochastic RMR survival curves tend to slightly overestimate the surviving fraction compared to deterministic results. But this is a very minor divergence and deterministic RMR survival curves approximate well the stochastic RMR survival curves.

At high LET other effects occur. First of all we note that the α/β ratio, given in Table I is the highest for cells irradiated with high LET radiation. This denotes a low sensitivity to dose fractionation. High LET radiation is actually much more damaging and induces locally multiple damage sites as explained earlier. Therefore after each formation of damage by high LET particles repair, enzymes are usually swamped making repair less efficient throughout the irradiation rendering the dose-fractionation effect less important with high LET radiation. We also observe equally good fits to the high LET data with the stochastic model, using CPP and CPP with chord length distribution, and deterministic model. The deterministic model was used with the VC software to get radiobiological parameters, but nevertheless using those deterministic parameters we obtained equally good fits between stochastic and non-stochastic results. The deterministic results can be used to fit high LET survival data by selecting a set of parameter values that compensate for the inadequate treatment of the stochastic aspects of damage formation and repair.

We can also compare the overall trends obtained by Sachs and Hlatky. (4). For low and high dose rates, and low and high LET radiation trends in the surviving fraction look similar to the ones we obtained in FIGS. 15 and 17. The Markov model used by Sachs and Hlatky and the CPP both produce the same general trends in survival curves.

Finally, we observe again in FIG. 17 that CPP with specific energy distribution underestimate surviving fraction. We see this for both low and high LET radiation and RMR parameters calculation should be reconsidered for this model. Another reason explaining the underestimation of the survival results is the shape of the DSB distribution with CPP using specific energy distribution. As we observed earlier in FIGS. 11 and 12 high levels of DSB occur more often if we consider specific energy distribution. Therefore this leads to overestimate the cell killing, and so underestimate the surviving fraction.

Dose rate sparing

FIG. 18 shows survival curve for a dose of 10 Gy, low LET radiation, and dose rate varying from 0.01 to 1000 Gy/h. Stochastic, and deterministic survival curves are shown in FIG. 18, as well as stochastic, and deterministic survival curves with the linear lethal misrepair term, ϕ , set to zero. As we saw previously the quadratic term in Eqs. (2,3) is the main source of discrepancies between stochastic and non-stochastic survival curves. Also, by setting the linear lethal misrepair term, ϕ , to zero, we can make comparison with the Monte Carlo calculation performed by Sachs and Hlatky (4).

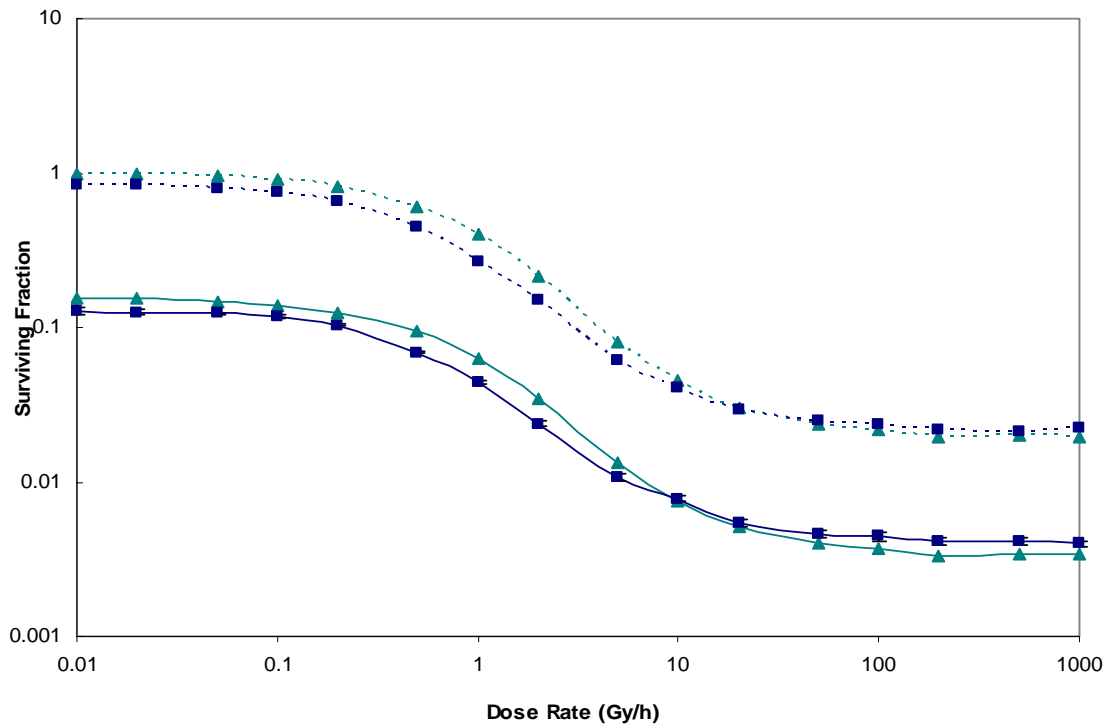


FIG. 18. Effects of fluctuations on dose rate sparing for low LET radiation, for cell line AG01522. All curves show surviving fraction vs. dose rate at a dose of 10Gy. (—) Surviving fraction predicted by the RMR model (--) Surviving fraction predicted by the RMR model with parameter ϕ set to 0. (▲) Surviving fraction predicted by the deterministic RMR model. (■) Surviving fraction predicted by the stochastic RMR model.

FIG. 18 looks similar to figures obtained by Sachs' calculations (4). Whether the linear lethal misrepair term, ϕ , is set to zero or not, it is generally found that stochastic approach predicts a decrease in the surviving fraction at low dose rates, while at high dose rates it has the opposite effect.

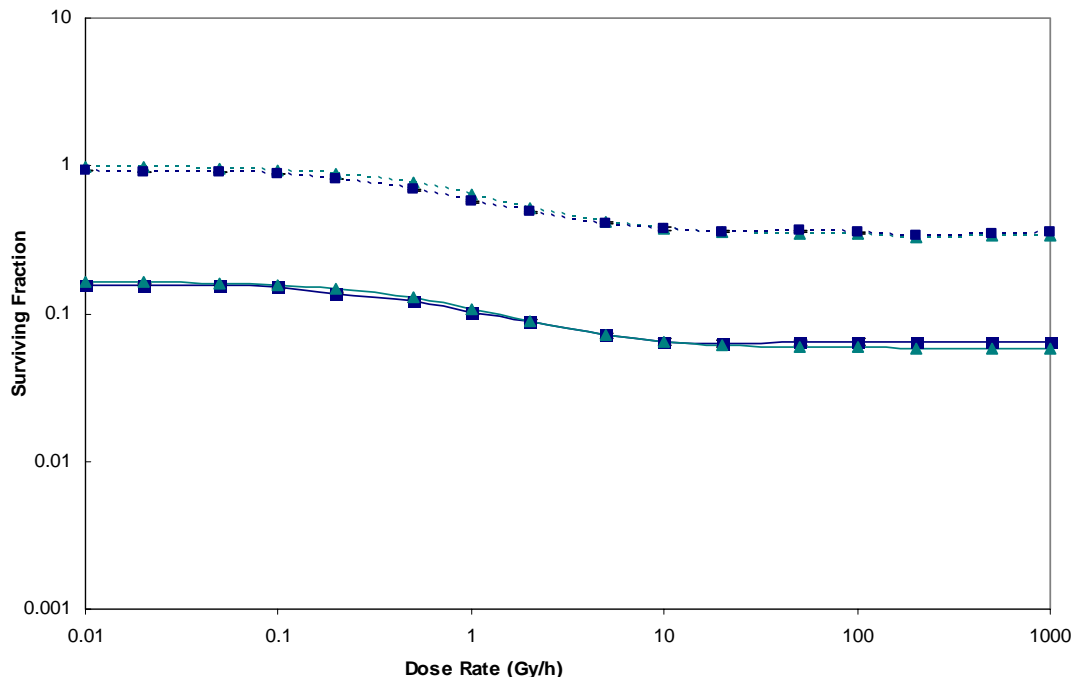


FIG. 19. Effects of fluctuations on dose rate sparing for high LET radiation, for cell line SQ20B. All curves show surviving fraction vs. dose rate at a dose of 10Gy. (—) Surviving fraction predicted by the RMR model (--) Surviving fraction predicted by the RMR model with parameter ϕ set to 0. (▲) Surviving fraction predicted by the deterministic RMR model. (■) Surviving fraction predicted by the stochastic RMR model.

Also, FIG. 19 presents survival curves for a dose of 10 Gy, for high LET radiation, and dose rate varying from 0.1 to 1000 Gy/h. The general pattern described above is still applicable, but to a lesser extent than before. There is a good fit between stochastic and non-stochastic results at low and high dose rates. However if we look at the plots given by Sachs et al. the discrepancy between stochastic and non-stochastic surviving fraction is greater than what we have in FIG. 18. This is because Sachs et al used non relevant parameters for high LET radiation that the discrepancy occurs (5). VC software selected radiobiological parameters fitting with high LET survival data. Parameters in the RMR model are then more appropriate for survival calculations for low and high dose rates.

Other dose sparing curves for cell lines A549, HeLa, HX118, and M10 are reported in FIG. 20. Cell lines A549, HeLa, and HX118 are given for low LET (^{60}Co gamma radiation). While cell line M10 is given for higher LET (15 MeV neutron).

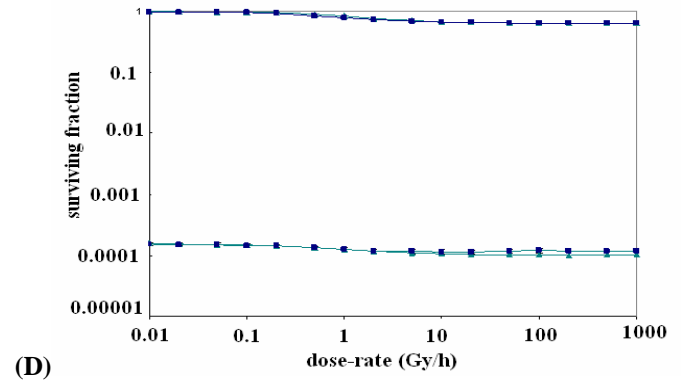
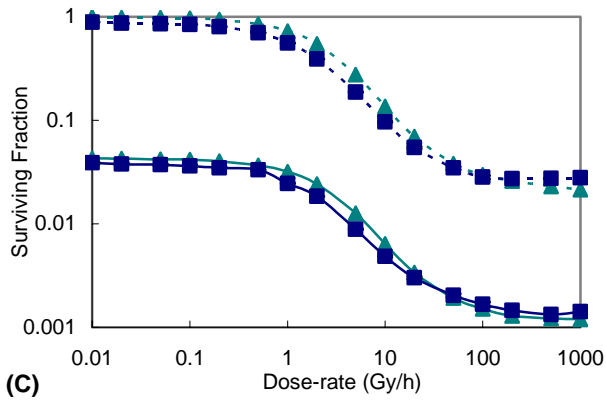
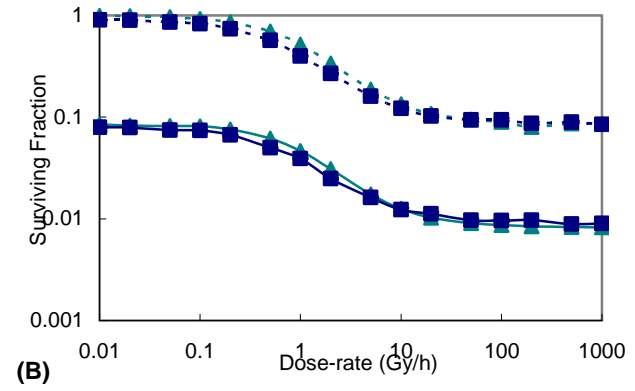
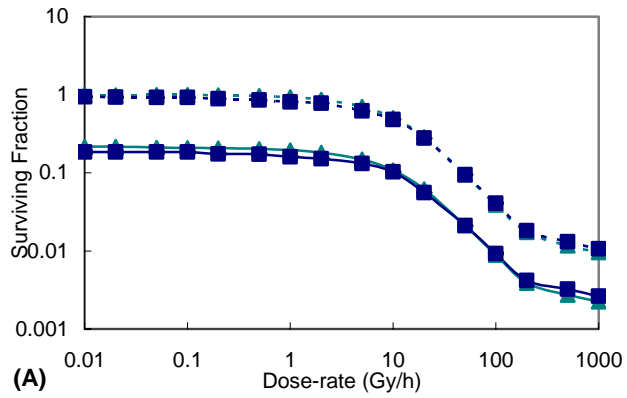


FIG. 20. Effects of fluctuations on dose rate sparing for several cell lines: (A) A549, (B) HeLa, (C) HX118, and (D) M10. All curves show surviving fraction vs. dose rate at a dose of 10Gy. (—) Surviving fraction predicted by the RMR model (- -) Surviving fraction predicted by the RMR model with parameter ϕ set to 0. (\blacktriangle) Surviving fraction predicted by the deterministic RMR model. (\blacksquare) Surviving fraction predicted by the stochastic RMR model. A, B, and C are for Co-60 exposures; D is for 15 MeV neutrons.

CONCLUSIONS

A stochastic DNA damage formation model was developed using Monte Carlo methods. Via a CPP, we computed distributions of the initial yields of DSB for low and high LET radiation. We have found that with low LET radiation the initial distribution of DSB almost follows a Poisson distribution. Exact means and variances have been calculated and compared with the first and second moment of Poisson distributions. Both results are similar. On the contrary, for high LET radiation, the initial distribution of DSB was found to deviate from a Poisson distribution. Although the means agree fairly well, the variance of the distribution of initial DSB generated with Monte Carlo is twice as great as the variance of the Poisson distribution. With increasing particle LET, the number of DSB per track traversing the cell nucleus increases, inducing clusters of DNA lesions. Compared with simple CPP we observed broader DSB distribution when adding chord length distribution in the model, and even broader spectrum yet when adding specific energy distribution. Although implementation of the chord length distribution is an improvement to the model, the DSB distribution stays very close with and without the chord length distribution. Implementation of specific energy distribution changes the shape of DSB distribution because it includes random processes such as secondary particles or energy loss straggling.

Then the main thrust of this work was to incorporate this stochastic DNA damage formation model, into stochastic RMR software aiming to simulate the repair and misrepair of DNA DSB. The endpoint of interest was the number of lethal lesions, that could be related to the surviving fraction of a cell population. To implement RMR model's differential equations, we develop a database of radiobiological parameters for various cell lines from survival experimental results found in literature using the VC software. Seven human cell line datasets from literature, with various sensitivities to radiation has been analyzed. Using the representative radiosensitivity parameters, we generated survival curves for various doses, dose rates, and particle LET.

A mathematical verification of the software was presented via simple case study, and the results were found to be consistent with simple analytical solutions.

We presented comparison of survival results for deterministic and stochastic models and we compared those calculated results with the measured ones. For low LET radiation and low dose rates we observed that deterministic results overestimate the surviving fraction compared to stochastic results obtained with CPP and CPP using chord length distribution, because, for any fluctuating variable the average of squares is greater than the square of the average. At high dose rates we saw that stochastic RMR model survival curve shows non-linearity at low doses, because of interactions of lesions produced by statistically independent tracks. For high LET radiation, stochastic and deterministic RMR survival curves agree fairly well at low doses and predict the same shoulder as initial slope of the survival curve. As dose increases we noted some discrepancies. These are very minor and deterministic RMR survival curves approximate the stochastic RMR survival curves. Deterministic results approximately match stochastic results when chord length distribution is included. Stochastic survival results obtained with CPP using specific energy distribution diverge from deterministic using parameter calculated by VC software and experimental results.

We studied the fluctuation in dose rate sparing for low and high LET radiation observing predicted surviving fraction at a dose of 10Gy vs. dose rate. Basically we saw that stochastic approaches, CPP and CPP with chord length distribution, predicted a decrease in the surviving fraction at low dose rates, while at high dose rates it has the opposite effect, although both approaches give very similar results.

Unlike past model intercomparison studies, we conclude that with good characteristic radiosensitivity parameters, divergences between deterministic and stochastic survival results are not that important when we consider CPP or CPP with chord length distribution. The VC software has proved to be a useful tool to provide input for RMR model using experimental datasets and to get good representative radiobiological parameters.

However, when we try to have a more realistic model, considering specific energy distribution, deterministic and stochastic models disagree on survival results.

Future efforts would include developing algebraic expressions and these could be used to summarize trends in radiosensitivity parameters as a function of particle LET. These algebraic expressions may provide some new insights into the biological basis for LET effects and provide data to help guide the design of radiation therapy treatment plans.

Divergence of stochastic results using CPP with specific energy distribution should be examined, and relevance of RMR parameters with this kind of stochastic model should be investigated. Also as more DSB are expected to be created as the particle LET increases, we could look into a model with a number of DSB created per Gray per tracks, Σ_{DSB} , varying with particle LET.

An improvement of the model would be to current model other cell death pathways processes such as apoptosis. There are many other possibilities for improvement of the current model and algorithm. Tumor response is governed by the four “Rs”, repair, repopulation, reoxygenation, and redistribution (35). It could be interesting to add some more features to our model rather than modeling only repair. Some models consider repopulation in their survival calculation. Reoxygenation and redistribution could also be implemented in the model to better account for all biological processes that could influence survival endpoints. Also as the cell is dividing we could take into account cell cycle effect, and the variation of radiosensitivity parameters throughout the cell cycle. Particle track structure could also be used to compute the specific energy deposition within a cell with Monte Carlo techniques.

REFERENCES

1. D.J. Brenner, L.R. Hlatky, P.J. Hahnfeldt, Y. Huang, and R.K. Sachs, The linear-quadratic model and most other common radiobiological models result in similar predictions of time-dose relationships. *Radiat. Res.* **150**, 83-91 (1998).
2. C.A. Tobias, The repair-misrepair model in radiobiology: comparison to other models. *Radiat. Res.* **8** (Suppl.) 77-95. (1985).
3. N. Albright, and A. Markov, formulation of the repair-misrepair model of cell survival. *Radiat Res.* **118**, 1-20 (1989).
4. R.K. Sachs, and L.R. Hlatky. Dose rate dependent stochastic effects in radiation cell-survival models. *Radiat Environ Biophys.* **29**, 169-84 (1990).
5. R.K. Sachs, L. Hlatky, P. Hahnfeldt, and P.L. Chen. Incorporating dose- rate effects in Markov radiation cell survival models. *Radiat. Res.* **124**, 216-226 (1990).
6. R. Iyer, and B.E. Lehnert, Effects of ionizing radiation in targeted and non-targeted cells. *Arch. Biochem. Biophys.* **376**,14-25. (2000).
7. J.D. Watson and F.H. Crick. The structure of DNA. *Cold Spring Harb Symp Quant. Biol.* **18**, 123-31 (1953).
8. J.P. Pouget, and S.J. Mather. General aspects of the cellular response to low and high LET radiation. *Eur J Nucl Med.* **28**, 541-561 (2001).
9. A. Lawen. Apoptosis-an introduction. *Bioessays.* **25**, 888-896. (2003).
10. F. Attix, Types and sources of ionizing radiation. In *Introduction to radiological physics and radiation dosimetry*, pp. 2-3. John Wiley & Sons, New York 1986.
11. R.D. Stewart. The Nature of a Fatal DNA Lesion. PNNL-SA-30810, June 25 2001
12. J.F. Ward, DNA damage produced by ionizing radiation in mammalian cells: identities, mechanisms of formation, and reparability. In *Progress in nucleic acid*

- research and molecular biology*. pp. 95-125. Academic Press, New York 1988.
13. J.F. Ward. The complexity of DNA damage: relevance to biological consequences. *Int J Radiat Biol.* **66**, 427-432 (1994).
 14. P.L., Olive. The role of DNA single- and double-strand breaks in cell killing by ionizing radiation. *Radiat. Res.* **150** (Suppl.), 42–51. (1998).
 15. L. Hlatky , R.K. Sachs, M. Vazquez, and M.N. Cornforth. Radiation-induced chromosome aberrations: insights gained from biophysical modeling. *Bioessays.* **24**, 714-723 (2002).
 16. R.K. Sachs, P. Hahnfeld, and D.J. Brenner. The link between low LET dose-response relations and the underlying kinetics of damage production/repair/misrepair. *Int J Radiat Biol.* **72**, 351-374 (1997).
 17. S.B. Curtis. Lethal and potentially lethal lesions induced by radiation--a unified repair model. *Radiat Res.* **106**, 252-270 (1986).
 18. R. Stewart, Two-lesion kinetic model of double-strand break rejoining and cell killing. *Radiat. Res.* **56**, 365-378 (2001).
 19. M.R. Lieber, Y. Ma, U. Pannicke, and K. Schwarz. Mechanism and regulation of human non-homologous DNA end-joining. *Nat Rev Mol Cell Biol.* **9**, 712-720 (2003).
 20. I. Radulescu, K. Elmroth, B. Stenerlow. Chromatin organization contributes to non-randomly distributed double-strand breaks after exposure to high LET radiation. *Radiat. Res.* **161**, 1-8 (2004).
 21. A.M. Kellerer, The CPP in microdosimetry. In *Fundamentals of microdosimetry* (B. Bjarngard and F. Attix Eds), pp 97-112. Academic Press, Orlando, FL 1985.
 22. R.G. Dale, The application of the linear-quadratic dose-effect equation to fractionated and protracted radiotherapy. *British Journal of Radiology*, **58**, 515-528 (1985).
 23. H.D. Thames. An ‘incomplete-repair’ model for survival after fractionated and continuous irradiations. *Int J Radiation Biology* **47**, 319-339 (1985).

24. D. Brenner, and E.J Hall, Fractionation and protraction for radiotherapy of prostate carcinoma, *Int J. Radiation Oncology Biol. Phys.* **43**, 1095-1101 (1999).
25. F.J. Sullivan, J. Carmichael, E. Glatstein, and J.B.Mitchell, Radiation biology of lung cancer. *Journal of Cellular Biochemistry* (Suppl.) **24**, 152-159 (1996).
26. E.J. Hall, M.J. Marchese, M.B. Astor, and T. Morse, Response of cells of human origin, normal and malignant to acute and low dose rate irradiation. *Int. J. Radiat. Onc. Biol. Phys.* **12**, 655-659 (1986).
27. O Algan, C.C. Stobbe, A.M. Helt, G.E. Hanks, and J.D. Chapman, Radiation inactivation of human prostate cancer cells: the role of apoptosis. *Radiat. Res.* **146**, 267-275 (1996).
28. G.G. Steel, J.M. Deacon, G.M. Duchesne, A. Horwich, L.R. Kelland, and J.H. Peacock, The dose rate effect in human tumor cells. *Radiotherapy and Oncology.* **9**, 299-310 (1987).
29. J.B. Mitchell, J.S. Bedford, and S.M. Bailey. Dose rate effects in mammalian cells in culture III. Comparison of cell killing and cell proliferation during continuous irradiation for six different cell lines. *Radiat Res.* **79**, 537-51 (1979).
30. M. Belli, D. Bettega, P. Calzolari, F. Cera, R. Cherubini, M. Dalla Vecchia, M. Durante, S. Favaretto, G. Gialanella, G. Grossi, R. Marchesini, G. Moschini, A. Piazzola, G. Poli, M. Pugliese, O. Saporà, P. Scampoli, G. Simone, E. Sorrentino, M.A. Tabocchini, L. Tallone, P. Tiveron, Inactivation of human normal and tumour cells irradiated with low energy protons. *Int J Radiat Biol.* **76**, 831-839. (2000).
31. R B. Hawkins, A microdosimetric-kinetic model for the effect of non-Poisson distribution of lethal lesions on the variation of RBE with LET. *Radiat. Res.* **160**, 61-69. (2003).
32. H. H Rossi, and M. Zaider, Microdosimetric quantities and their moments. In *Microdosimetry and its applications*, pp. 17-27. Springer-Verlag, Berlin, 1996.
33. ICRU, Microdosimetry Report #36, ICRU, Bethesda, MD 1983.

34. E. J. Hall, Repair of radiation damage and the dose rate effect, In *Radiobiology for the radiologist*, pp.67-88. Lippincott Williams & Wilkins, Philadelphia, 2000.
35. S.B Curtis, Mechanistic models, *Basic Life Sciences*. **58**, 367-382 (1991).

VITA

Julien Partouche was born on July 28, 1978 to Roger Partouche and Jacqueline Partouche in Chenôve (21), France. He graduated from Lycée de Semur-en-Auxois option Scientifique. He received his of Diploma of engineering, Bachelor of Science in Mathematics and Physics from Fondation EPF, Sceaux in May 2002. His permanent address is 7 square Port Royal, 75013 Paris, France.